2mif

X-660-74-198
PREPRINT

ENERGETIC PARTICLES IN THE JOVIAN MAGNETOSPHERE

J. H. TRAINOR
F. B. McDONALD
B. J. TEEGARDEN
W. R. WEBBER
E. C. ROELOF

JUNE 1974

GODDARD SPACE FLIGHT CENTER
GREENBELT, MARYLAND

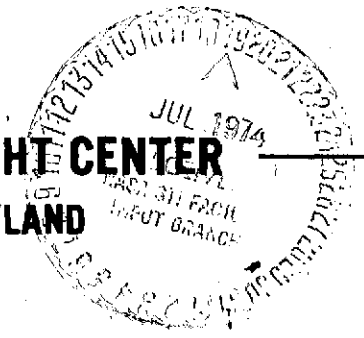

ENERGETIC PARTICLES IN THE JOVIAN MAGNETOSPHERE

J.H. Trainor, F.B. McDonald, and B.J. Teegarden
Laboratory for High Energy Astrophysics
NASA/Goddard Space Flight Center
Greenbelt, Maryland 20771

and

W.R. Webber and E.C. Roelof
Department of Physics
University of New Hampshire
Durham, New Hampshire 03824

ABSTRACT

This paper presents a detailed account of the Pioneer 10 encounter with Jupiter as viewed by the Goddard/Univ. of New Hampshire Cosmic Ray Experiment. Flux time histories of electrons and protons are given over a wide energy band. These show a marked variation with magnetic latitude. Significant removal of low energy protons by Io is apparent in the inner magnetosphere ($\lesssim 6\ R_J$). Proton and electron energy spectra are given at various Jovicentric distances. The electron spectra are remarkably hard and constant in slope in the .12-8.0 MeV interval, the electron spectral index having a value of 1.5-2.0 in the region outside 25 R_J. Proton spectra are shown to transform from a power law with indices in the 3-4.2 range to more nearly exponential forms in the inner regions ($\lesssim 40\ R_J$). Extensive data are presented on the angular distributions of protons and electrons at various locations in the Jovicentric magnetosphere. In addition, a harmonic analysis of 1-2 MeV proton angular distributions has been performed. Simple co-rotation is shown to exist out to $\sim 23\ R_J$. Beyond this point other effects are contributing significantly to the particle anisotropies. Alpha/proton ratios are given as a function of Jovian radius and are compared to the earth and solar wind values.

ENERGETIC PARTICLES IN THE JOVIAN MAGNETOSPHERE

I. INTRODUCTION

In this paper we provide a detailed account of the experimental observations of the Jovian magnetosphere made by the Goddard/Univ. of New Hampshire Pioneer 10 cosmic-ray experiment. Additional interpretive papers on this data will follow at a later date. An informative series of preliminary papers concerning the Jovian magnetosphere has appeared in Science (Fillius et al., 1974; Simpson et al., 1974; Smith et al., 1974; Trainor et al., 1974; and Van Allen et al., 1974). This experiment consists of a set of three solid-state telescopes, each designed to compliment the others and to cover a broad range in energy, intensity and charge spectra. The three telescopes are shown schematically in Figure 1; they are: 1) the High-Energy Telescope (HET), 2) Low-energy Telescope (LET-I), and 3) Low-Energy Telescope-II (LET-II). The HET and LET-I are designed primarily for measuring the relatively low fluxes of cosmic rays in interplanetary space. As such their geometry factors are relatively large and they cannot tolerate fluxes $\gtrsim 2 \times 10^5/cm^2$-sec-ster. Their usefulness is, therefore, limited to the outer regions of the Jovian magnetosphere ($\gtrsim 20\ R_J$). They are, however, high resolution double dE/dX vs. E instruments that provide unambiguous particle identification and precise energy spectra so that their contribution to the overall body of data is quite significant.

The LET-II telescope was designed to measure low-energy solar flare particles in interplanetary space and trapped particles in the Jovian magnetosphere. It has a relatively small geometry factor (1.5×10^{-2} cm^2-ster), and can readily measure fluxes up to $\sim 4 \times 10^6/cm^2$-sec-ster. It is surrounded by an aluminum and lead shield which will stop electrons up to $\sim$25 MeV and protons to $\sim$140 MeV. The telescope employs a two-

parameter analysis technique to separate electrons and protons. The front element SI has an electronic threshold which is set such that any electron penetrating to SII is below threshold and any proton penetrating to SII is above threshold. Selected counting rates in all three telescopes are divided into eight angular sectors to measure particle anisotropies.

A major effort has been devoted to understanding the response of all detector systems in the presence of intense particle fluxes. The onset of saturation in the LET-I and HET systems is abrupt and well defined. Negligible corrections are necessary prior to this saturation point. As will be discussed in the Appendix, the LET-II corrections are more complex. However, the response is now sufficiently well understood so that the 1-2 MeV and 14-21 MeV proton fluxes can be determined over the complete trajectory.

There is significant overlap in the response functions of the three telescopes, and it was of great value to observe the consistency between flux measurements made with completely different detector systems. For example, the LET-I and LET-II proton data in the .5-2 MeV region are in excellent agreement from 100-16 R_J. This is especially helpful in the outer Jovian Magnetosphere where the nuclear component is small (1-10%) compared to electrons of the same energy. Furthermore, LET-I provides a very sensitive measurement of protons and alphas in the 3-20 MeV range down to a sensitivity of 10^{-3} protons/cm-sec-ster MeV up to $\sim 20\ R_J$. A complete description of this instrument will be published in the IEEE Transactions on Nuclear Science (Stilwell et al., 1975). The

energy and charge ranges of each telescope are summarized in Table 1.

Figures 2 and 3 give an overview of the Jovian electron and proton fluxes as observed by the experiment, showing particle energies near the upper and lower ranges of the instrument. In discussing these observations, it is convenient to divide the Jovian magnetosphere into 4 regions:

1) The region outside the Jovian magnetosphere in which large fluxes of MeV electrons and protons are observed to be coming from the magnetosphere: The MeV electrons are seen at distances of 1 AU away from Jupiter. These are described in a companion paper (Teegarden et al., 1974) which shows that, in fact, Jovian electrons have been a major contributor to the 3-20 MeV electron flux measured at earth. A steady increase in the flux of > 0.5 MeV protons was also observed ~ 5 R_J before the crossing of the bow shock. These are probably also present at much greater distances from Jupiter but at a much smaller intensity than that displayed by the electrons.

2) The outer Jovian magnetosphere: This region extends from the bow shock crossing (109 R_J) to ~ 50 R_J. The magnetic field is ~ 8-20γ and like the earth's tail is dominated by a neutral plasma sheath which is drawing the field lines outward. It is a region of quasi-trapping and diffusion. Both the electrons and protons show remarkably constant energy spectra, $E^{-\gamma}$ with $\gamma = 1.5$-2.0 and 4 respectively. This suggests that almost no acceleration occurs in this region. There are rapid changes in flux and angular distributions. The high energy electrons (i.e. > 6 MeV) show a reasonable 10 hour periodicity as

expected since the nominal magnetic latitude of the spacecraft should vary with the rotation period of the planet (∿10 hrs). This is not nearly as significant for the protons or for the lower energy electrons. The changes in the proton and electron flux are frequently uncorrelated.

3) The region between ∿50 to 25 R_J is one of transition between the outer diffusion zone and the point where the field rigidly rotates with the planet. The proton energy spectra begin to change from a power law to an exponential energy form on a gradual scale suggesting that some acceleration is occurring. The angular distribution of the protons display large (up to ∿70%) anisotropies and the hinging effect produced by the transition is strongly evident. The magnetic field is still changing rather slowly and it is not clear if the particles are stably trapped.

4) Inside 25 R_J: The particle angular distributions indicate that the field lines are rigidly rotating with the planet within ∿25 R_J, and this may mark the outer boundary for really stable trapping. This rapid decrease in the co-rotation anisotropy provides further evidence that the proton spectra are becoming increasingly flat below 1 MeV. At the outer edge of this region there is a significant increase in the 1.2-2.1 MeV (Fig. 3) proton component which climbs steadily until 6 R_J. Inside 6 R_J the proton component is strongly attenuated by the presence of the Jovian moon, Io. For example the 1-2 MeV component is reduced by a factor of 60 by Io absorption. The flux of all proton components then increases until ∿0115 on Dec. 4, when the spacecraft crossed the magnetic equator at 3.5 R_J.

The outbound trajectory (Fig. 2 & 3) near the dawn meridian was

strikingly different from the inbound span in many respects. The peak fluxes are near the predicted magnetic equator; however, the dominant feature is the 10-hour periodicity which produces peak-to-valley ratios of as much as 5 decades for a 20° excursion in latitude. This implies that both electrons and protons are much more concentrated in the low latitude region on the outbound pass.

2. ELECTRON AND PROTON SPECTRA

Figures 4 and 5 show the differential electron spectra measured near the magnetic equator by the HET and LET-II telescopes on the inbound and outbound passes, respectively. The spectra in this energy range are remarkably hard and similar over the region outside $\sim$25 R_J where we have measurements. The spectra are actually slightly harder in the outermost regions and, as reported in the companion paper (Teegarden et al., 1974), are very similar to the spectra of electrons leaking from the Jovian magnetosphere and measured on Pioneer 10 many months before encounter. This, of course, is quite different from the behavior in the earth's radiation belts. We have found no obvious correlation between the spectra shape in the .12-8.0 MeV region and magnetic latitude.

Figure 6(a) through 6(g) show proton spectra measured by our LET-I and LET-II telescopes in the energy region between 100 KeV and 21 MeV. The data from the magnetosheath region and from the radiation belts in to $\sim$40 R_J seem to be well fitted by a simple power law with an exponent of $\sim$4 but varying from 4.2-3.0 for brief periods. We interpret this as indicating very little acceleration occurs in the outer magnetosphere.

Beginning with the measurements inside ~ 41 R_J the spectra are better fitted by an exponential than a power law. Note that the one data point plotted at 10^6 in Figure 6(d) has been arbitrarily plotted there, since it would have fallen above a flux of $10^6/cm^2$-ster-sec-MeV, and a correction is required for LET-II data above that figure. None of the LET-II data shown requires a correction of any kind. The spectra near 22 R_J and 15 R_J show a similar exponential form. Note in Figure 6(f) that two LET-II data points are now in the non-linear region and therefore are not used. Similarly in Figure 6(f) one can see that the LET-I telescope with its much larger geometrical factor and lack of shielding has now become saturated and the apparent count rates have fallen. Figure 6(g) for comparison shows the spectra taken in the first flux minimm outbound in the region 12.6-13.5 R_J. It is well fitted by a power law of exponent 3.5.

3. JOVIAN ALPHA PARTICLES

Unambiguous alpha particle identification was obtained in the 3.2-5.6 MeV/nuc interval using two-parameter analysis in the LET-I telescope. The alpha particle flux in this energy range was quite small in the outer Jovian magnetosphere, making it necessary to average data over fairly long time periods to obtain reasonable statistics. Figure 7 shows the ratio of alpha and proton intensities as a function of Jovian radius for the inbound pass of Pioneer 10. A general decreasing trend in the ratio is apparent with one exception, the point between 40 and 55 R_J. This point, however, occurs at the time when Pioneer 10 reentered the magnetosheath (Wolfe et al., 1974a). The abnormally high value of the point suggests that conditions near the boundary of the

magnetosphere prevailed during this time and is, therefore, quite consistent with Wolfe et al.'s (1974b) observations. The ratio varies between $\sim 6 \times 10^{-3}$ and $\sim 6 \times 10^{-4}$ over the region measured. This is to be compared with the solar wind α/p ratio which varies over the range .01-.1 (see, for example, Wolfe et al., 1966; Gosling et al., 1967). Thus the α/p ratio in the outer part of the Jovian magnetosphere is closest to the solar wind values.

The α/p ratio in the earth's magnetosphere shows little L dependence but apparently has a very strong latitude dependence (D.J. Williams, private communication). The value of the ratio at earth spans the range 10^{-2} - 10^{-4}. With the limited statistical accuracy of our data it is difficult to establish whether a strong latitude dependence exists. The earth observations, however, were made in regions where particles are stably trapped, and such is almost certainly not the case for the measurements presented here.

4. PROTON AND ELECTRON ANGULAR DISTRIBUTIONS

Figures 8 through 11 sample the angular distributions measured for two of our logical rates from the LET-II telescope, showing hourly average data for .49-2.15 MeV protons and .78-1.0 MeV electrons. In the outermost regions of the magnetosphere anisotropies are present and variable in both the electrons and protons. By the time one reaches $\sim 70 R_J$ (Fig. 8), the electrons have already settled down to a nearly isotropic behavior, but the protons are still quite variable as to the magnitude and direction of the anisotropy. The direction of the anisotropy is generally correct for the co-rotation effect which should be from the left of the figures. Figure 9 illustrates data from 40 to 35 R_J showing that the electrons have become even more isotropic, and the proton

distributions have settled down to a pattern more regular in amplitude and direction. The rocking of the distribution due to the 10-hour periodicity in the magnetic field is quite clear.

Figure 10 illustrates data from 25 R_J to 19 R_J. The proton distributions show a well defined, stable anisotropy from the co-rotation direction. The electrons at the beginning and end of the period show an extremely isotropic behavior; however, there is a huge double-ended anisotropy seen as we approach the expected location of the magnetic equator (See Figure 2). This anisotropy smoothly came and went over a period of almost 4 hours and was aligned along the magnetic lines.

The out-bound data covered in this paper is summarized in Fig. 11. These data are all taken near the flux maxima in 10-hour periodicity so strongly apparent in the outbound data. Small anisotropies are commonly seen in the electron data, most often a double-ended distribution, and presumably at the location of the magnetic equator. The protons generally show a behavior similar to the inbound pass, except, of course, that the sense of the co-rotational effect is from the right now. In the data shown here outside 30 R_J, more variation in direction is noted outbound than inbound at the same distance, and the proton distribution shown near 47 R_J is most unusual. The co-rotational effect is being completely masked. This behavior began after $\sim$ 1400 UT and persisted for several hours, again while the spacecraft was apparently near the magnetic equator.

5. HARMONIC ANALYSIS OF PROTON ANGULAR DISTRIBUTIONS

The great extent of the Jovian magnetosphere combined with the relatively short rotation period means that co-rotation anisotropies

should be an important aspect of the particle angular distributions. Furthermore, the weak, non-dipole Jovian magnetic field in the 50 - 25 R_J region ($\sim$20Y) suggests that anisotropies produced by particle intensity gradients may be significant. A number of rates from the three detector systems were sectored into 8 different bins for each spacecraft rotation and then were summed over 5 rotations. In this section we will be concerned with the LET-II data for the proton energy intervals 1.2-2.15 MeV. In addition there were 4 electron intervals extending between .1 and 2 MeV.

The opening angle of the LET-II (30°) is small compared to the 45° sector width so no deconvolution of the data is required. A harmonic analysis of the form

$$J(\theta) = A_o + A_1 \sin(\theta - \theta_1) + A_2 \sin 2(\theta - \theta_2)$$

was performed on the 3600 sec averages. The resulting values for A_1/A_o, θ_1 and A_2/A_o for the 1.2-2.2 MeV interval are shown in Figures 12, 13 and 14. Examining the plot of θ_1, there are large systematic fluctuations which steadily decrease and at 23 R_J there is a well-defined "hinge point" with the particles coming from the direction $\theta_1 \sim 90°$ as one might expect. Inside this point there would appear to be rigid rotation of the field with the rotation of the planet. Thus 23 R_J is probably an upper limit on the region of durable trapping. This is also the point where there is a steady increase in the 14-21 MeV proton flux. We have not completed the analysis of the variation of θ_1 in the transition region between 50 and 25 R_J. This region is obviously "hinged" between the outer diffusion region and that of rigid rotation. However, there are probably other effects present. The changes observed in the low-energy (.4-1 MeV) proton spectra suggest the particles in this region

are being accelerated at a very slow rate.

A_1/A_0 is a measure of the first order anisotropy. The expected co-rotation anisotropy is given by

$$\xi = \frac{f(v_1) - f(v_2)}{f(v_1) + f(v_2)}$$

$$v_1 = V_r + v$$

$$v_2 = V_r - v$$

where $f(v) \propto \frac{J(E)}{E}$ is the non-relativistic particle distribution function, v is the particle velocity and $V_r = \omega r$ is the rotation velocity.

For power-law spectra this is of the form

$$\xi = \frac{E_2^{\gamma+1} - E_1^{\gamma+1}}{E_2^{\gamma+1} + E_1^{\gamma+1}}$$

and for $\gamma = 4$ this reduces to

$$\frac{(v + V)^{10} - (v - V)^{10}}{(v + V)^{10} + (v - V)^{10}}$$

For the 1.2 - 2.2 MeV region $\bar{E} \approx 1.4$ MeV; $v = 1.6 \times 10^7$m/sec; $V_r = 12.6\ N \times 10^3$, where N is the distance to the observing point measured in units of R_J ($= 7.137 \times 10^7$m). At 25 R_J, $V_r = 3 \times 10^6$m/sec; $V_r/v = .019$; $\xi = 18\%$; at 50 R_J this increases to 37%. The expected co-rotation anisotropy for $\gamma = 4$ is shown as a dashed line in Fig. 12. The agreement with the innermost values of A_1/A_0 is good. The larger peaks of A_1/A_0 between 25 and 50 R_J are not understood. At 25 R_J the magnetic field is $\sim 20\gamma$ and the gyroradius of a 1.4 MeV proton is 12×10^8m. A gradient anisotropy of the order of $\frac{1}{R}\frac{dJ}{dR}$ is expected. This means that 100% increases per Jovian Radii would give an anisotropy of $\sim$ 20% in the same direction as the co-rotating anisotropy for negative values of dJ/dR (i.e. value of J increasing with decreasing R_J). This

may be the explanation for the large increases in A_1/A_0 which more closely coincide with minima in the particle intensity. For smaller values of v/V_r, A_1/A_0 reduces to the Compton-Getting factor

$\xi = (2 + \alpha\gamma)\, v/V_r$ where α is the following function of energy

$$\alpha = \frac{T + 2m_0c^2}{T + m_0c^2}$$

For electrons the smaller value of α and γ and the smaller value of v/V_r all combine to make the 0.5 MeV electron co-rotation anisotropy $\sim$ 30 times smaller than that of the protons and explain the difference generally observed between the two components.

The second harmonic A_2/A_0 is shown in Figure 14. The peaks anti-correlate with the A_1/A_0 peaks and coincide with the intensity maxima observed at or near the Jovian magnetic equator. This suggests a more stable population exists at this point.

6. PROTONS INSIDE $10R_J$

Protons in the inner region are treated separately in this section since the extremely high flux rates inside $10R_J$ have caused the detector response to enter a non-linear regime and significant corrections are required. These corrections are discussed in detail in the Appendix. Proton count-rate data from 1830 UT on December 3 to 1130 on December 4 are shown in Fig. 15 for the 1.2 to 2.15 MeV protons and 14.8 to 21.2 MeV protons where the curves shown are derived from averages over 144 seconds. These two energies were chosen since they correspond to relatively large energy losses respectively in the SI and SII elements of the LET-II telescope (see Fig. 1). The electron efficiencies for these counting rates are consequently quite small. Also shown in Fig. 15 are the angular distributions for 1.2-2.15 MeV protons from data averaged over

15 minutes.

The angular distributions shown in Fig. 15 for the 1.2 to 2.15 MeV protons are most interesting. The spacecraft was at ~ 20°S magnetic latitude at ~ 1730 and moving inbound towards the magnetic equator which it crossed at ~ 0100 on December 4. On the outbound leg, we reach a maximum northerly latitude of ~ 20° at ~ 0500 and return to near the equator at ~ 1000 on December 4. A small anisotropy, undoubtedly due to corotation, exists for many hours, up to ~ 1900 on December 3. Then as the spacecraft moves towards the equator (2000-2130) a small double-ended anisotropy appears with maxima perpendicular to the field lines. (It is difficult to see this effect in Fig. 15 due to the photographic reduction.) From our detailed data, this situation has clearly ended by 2230, going over to an X-type distribution from 2300 to 2330, and evolving in a complicated fashion to a bi-lobed distribution near the magnetic equator. The outbound data is the inverse of the above, with the exception that the anisotropies are larger at later times since the spacecraft is much nearer the equator.

Two important conclusions are obvious. As one moves across Io's orbit and observes a flux drop of a factor of 60, the angular distribution of the particles changes very little, although it is apparent that there is a small preference for Io removing particles with smaller pitch angles. Inside the orbit of Io, as the flux in this energy interval increases, it is apparent that particles are at first preferentially added at small pitch angles for a period of 30-45 minutes, and then preferentially at large pitch angles as the spacecraft moves towards the crossing

of the magnetic equator. Outbound the inverse sequence is true.

There are several features of the flux curves of Fig. 15 which deserve comment. The most obvious is the huge effect of Io in removing protons in the $\sim$ 1 MeV range. Had the effect not occurred, one could speculate that the flux of these protons could have been $\sim 10^{10}(cm^2 sec)^{-1}$ at $\sim$ 0100 on Dec. 4. Long before encounter several authors (Mead and Hess, 1974; Birmingham et al., 1974) had predicted the sweeping effect of the Jovian moons. While the effects do occur, in detail they are quite different from the predictions, depending upon the moon and the energy range. A later work (Hess et al., 1974) improves on the earlier work. Differences in detail, however, still exist.

The shape and size of the Io effect is quite similar inbound and outbound, although the spacecraft was leading Io in its orbit by less than 90° inbound and by more than 180° outbound. It thus appears that there is little azimuthal dependence of the effect for the 1.2-2.15 MeV protons and only a small one for the 14.8-21.2 MeV protons. These higher energy protons do show a smaller but clear signature in crossing the orbit of Europa inbound and outbound, although the magnitude appears to be somewhat different in the two cases. In the lower energy protons, there is a small effect at Europa inbound when the spacecraft was well off the equator and no observable effect outbound near the equator. These observations are quite consistent, since one expects the moons to have a smaller effect on particles which are mirroring near the equator.

Simpson et al. (1974), have pointed out a small latitude effect for the > 35 MeV protons. Those protons showed very strong maxima near $L \sim 3.6\ R_J$. The first peak was largest and occurred essentially

at the magnetic equator while the second peak occurred at $\sim 15°N$. Our data for the lower energy protons show a maximum in the flux at $\sim$ 0100 on Dec. 4, near the magnetic equator, but not the striking maximum shown in the $>$ 35 MeV data. However, on the outbound trajectory both of our lower energy proton fluxes show slight maxima at the time of the second peak reported by Simpson et al. (1974).

The fluxes of protons measured by this instrument inside the crossing of the magnetic equator continue to fall off, but it is obvious from the fluxes at $\sim$ 0100 and $\sim$ 0330 when the spacecraft was at $L \sim 3.6$ that the latitude dependence is not large over the latitude range covered by Pioneer 10. The decrease in fluxes inbound to periapsis may well be due to the effects of Amalthea, which orbits at 2.55 R_J. Apparently due to diffusion, the effects of particle removal by Io were seen at least 1 R_J outside the orbit of Io. A similar effect may indeed be present due to Amalthea.

The Pioneer 11 spacecraft will encounter Jupiter in early December, 1974. Two advantages of its trajectory are the high latitude region covered and the very close approach to the planet. One should learn a great deal more about this most interesting inner region if the spacecraft survives.

APPENDIX: DETECTOR RESPONSE IN HIGH FLUX REGIONS

We shall first discuss the problem of high rates in the logical anti-elements, SIIa and SIII, which form the anti-cup around SII. At the peak of the electron fluxes near ~0100 on Dec 4 these detectors were truly counting a few million counts per second. At count rates less than 5×10^4 counts/sec in the anti-elements, the system logic works as intended; however, at very high count rates, the dead time of a given threshold circuit, coincidence circuit or anticoincidence circuit becomes appreciable compared with the average time between true events. (Circuit dead time is here defined as the time after one event has been completed before another event can be recognized.) In effect, the anti-circuitry leaks at high count rates, and the leakage actually approaches asymptotic values of 15% to 30% depending upon pulse height. Thus, as one moves into the inner regions of the Jovian magnetosphere (inside about 10 R_J), a correction term is needed for the 14.8 to 21.2 MeV protons which depends upon the anti-element count rates.

The lower energy protons are logically selected as $SI(8)\overline{SII}\,\overline{SIIa}\,\overline{SIII}$ and are subject to a similar correction term as the higher energy protons. The SI(8) refers to the highest level threshold on SI of 1.2 MeV. From ground tests with random pulses and accelerator tests, we came to expect a maximum correction factor of ~5 in the region inside ~8 R_J. With an apparent count rate of $\sim 10^4$ counts per second just outside Io, this

would lead to a "true" count rate of $\sim 5 \times 10^4$ counts/sec, and by the performance data shown in Figure A1, a further correction (maximum factor of 1.4) would be needed for this effect, resulting in a net correction factor of ~ 7.

We were also able to calculate a value for the correction factors in two other ways from the data itself, using the angular distributions such as plotted in Figure 15 and the count rate saturation properties as shown in Figure A1. There is a small anisotropy apparent in the plots before and after passing through the count rate peaks just outside Io, but the distribution is nearly isotropic in the 15 minute interval while passing through the peak fluxes. If one assumes the distribution really is intermediate in anisotropy to that measured before and after the peak, then one can use the saturation properties from Figure 15 to arrive at the true distributions and count rates, and thus also the correction factors. For this case, the calculation resulted in a total correction factor of 7.4 in good agreement with the previous estimate of the anti-rate correction with a superimposed count rate correction.

The second method involves using the angular distributions of two different energy levels of SI while there is a good anisotropy present and when one is very certain that one distribution needs no count rate correction due to saturation effects, and the other distribution does need a substantial correction. In the period 2300 to 2400 on December 3, SI(8) (1.2-2.15 MeV) was showing a marked anisotropy while SI(7) (.78-2.15 MeV) showed a similar but smaller effect and

SI(6) (.49-2.15 MeV) showed the inverse of SI(8). The count rate in SI(6) was ~250 times that in SI(8) and would require a correction for count-rate saturation while SI(8) at ~400 cts/sec would require no count-rate correction. If one assumes that the SI(6) distribution should be the same as the SI(8) distribution, then using the data of Figure A1, one can calculate the true rates and the apparent rates sector-by-sector for SI(6), and by comparing the true apparent rate with the measured apparent rate, arrive at the value of the correction factor for the anti-element term. This should be the same for SI(6) and SI(8). The calculation for the period 2300-2400 on December 3 results in a value of 6.9 for this factor, again in fair agreement with the estimates from ground test. Similar calculations hourly through 0400 result in correction factors ranging from 5.3 to 3.2.

The smaller correction factors are associated with the peak count rates around 0115 where the true count rates for SI(6) were $\sim 6 \times 10^5$ counts/second. There is a larger uncertainty in these smaller factors due to the fact that one is in a region where the SI(6) apparent rates are rolling over rapidly while going into saturation.

Since the ground testing and the two different inflight methods all arrive at correction factors which agree within 50% of one-another we are able to construct a multiplicative correction curve for SI(8) ranging from 1.0 at 1700 on December 3, to 7.5 at 2112, to 6 at 22.2, to 7 at 0112, to 6 at 0600, to 7.5 at 0700, to 6 at 1000, and finally to 1 at 1300 on December 4. Using this correction curve, the count

rates of Figure 14 are converted to the fluxes shown in Figure A2. The uncertainty in these proton fluxes is due entirely to the uncertainty in the correction factor and we estimate this to be less than a factor of 2.

REFERENCES

Birmingham, T., W. Hess, T. Northrup, R. Baxter and M. Lojko, "The Electron Diffusion Coefficient in Jupiter's Magnetosphere," J. Geophys. Res. 79, 87, 1974.

Fillius, R.W., and C.E. McIlwain, "Radiation Belts of Jupiter," Science 183, 314, 1974.

Gosling, J.T., J.R. Ashbridge, S.J. Bame, A.J. Hundhausen, and I.B. Strong, "Measurements of the Interplanetary Solar Wind during the Large Geomagnetic Storm of April 17-18, 1965," J. Geophys. Res., 72, 1813.

Hess, W.N., T.J. Birmingham, and G.D. Mead, "Absorption of Trapped Particles by Jupiter's Moons," preprint, March 1974.

Mead, G.D., Private Communication to all Pioneer 10 experimenters, October 1973.

Mead, G.D. and W.N. Hess, "Jupiter's Radiation Belt and the Sweeping Effect of its Satellites," J. Geophys. Res. 78, 2793, 1973.

Simpson, J.A., D. Hamilton, G. Lentz, R.B. McKibben, A. Mogro-Campero, M. Perkins, K.R. Pyle, A.J. Tuzzolino, "Protons and Electrons in Jupiter's Magnetic Field: Results from the University of Chicago Experiment on Pioneer 10," Science 183, 306, 1974.

Smith, E.J., L. Davis, Jr., D.E. Jones, D.S. Colburn, P.J. Coleman, Jr., P. Dyal, C.P. Sonett, "Magnetic Field of Jupiter and its Interaction with the Solar Wind," Science 183, 305, 1974.

Stilwell, D.E., R.M. Joyce, J.H. Trainor, H.P. White, Jr., G. Streeter and J. Bernstein, "The Pioneer 10/11 and Helios A/B Cosmic Ray Instruments," to be published IEEE Trans. Nuclear Science NS-22 Feb. 1975.

Teegarden, B.J., F.B. McDonald, J.H. Trainor, W.R. Webber, and E.C. Roelof, "Jovian Electrons in Interplanetary Space," to be published in J. Geophys. Res.

Trainor, J.H., B.J. Teegarden, D.E. Stilwell, F.B. McDonald, E.C. Roelof, W.R. Webber, "Energetic Particle Population in the Jovian Magnetosphere: A Preliminary Note," Science 183, 311.

Van Allen, J.A., D.N. Baker, B.A. Randall, M.F. Thomsen, D.D. Sentman, H.R. Flindt, Energetic Electrons in the Magnetosphere of Jupiter," Science 183, 309, 1974

Wolfe, J.H., R.W. Silva, D.D. McKibbin, and R. H. Mason, "The Compositional, Anisotropic and Non-radial Flow Characteristics of the Solar Wind," J. Geophys. Res., 71, 3329, 1966.

Wolfe, J.H., Memorandum to Pioneer 10 Particle and Fields Experimenters, October, 1973.

Wolfe, J.H., H.R. Collard, J.D. Mihalov, "Preliminary Pioneer 10 Encounter Results from the Ames Research Center Plasma Analyzer Experiment," Science 183, 303, 1974.

ACKNOWLEDGEMENTS

The authors wish to acknowledge the excellent engineering support provided by Messrs. Stilwell, Joyce, White, Streeter and Beazley, which has been responsible for the superior performance of the experiment during the entire flight of Pioneer 10. We appreciate the assistance of the Pioneer Project Office of the Ames Research Center, NASA, especially that of Thomas Wong and Joseph Lepetich.

FIGURE CAPTIONS

1. Schematic drawing of the solid-state detector telescopes.

2. Electron time histories during the Pioneer 10 Jovian encounter. Angular distributions are given for selected time periods. Tick marks show points at which Pioneer 10 was predicted to be closest to the magnetic equator, based upon a rigidly rotating field due to a tilted dipole.

3. Proton time histories in two different energy intervals. Times of crossing of the orbits of the innermost Galilean satellites are shown respectively as JI, JII and JIII.

4. Electron differential energy spectra on the inbound pass of Pioneer 10 at three different values of RJ.

5. Electron differential energy spectra on the outbound pass of Pioneer 10 at three different values of RJ.

6. (a)-(g) Proton differential energy spectra at different values of Jovian radius.

7. Alpha-to-proton flux ratio as a function of Jovian radius. Ratio is taken for equal values of energy/nucleon.

8. Polar plots of angular distributions of proton and electron counting rates. Top of the figure is towards north ecliptic pole. The normal out of page is in direction of spacecraft spin axis.

9. Polar plots of angular distributions of proton and electron counting rates. Orientation of plots is the same as in Figure 8.

10. Polar plots of angular distributions of proton and electron counting rates. Orientation of plots is the same as in Fig. 8.

11. Polar plots of angular distributions of proton and electron counting rates. Orientation of plots is the same as in Figure 8.

12. Magnitude of the first harmonic of the proton 1.2-2.15 MeV angular distribution as a function of time and Jovian radius; dashed line indicates magnitude of anisotropy predicted from co-rotation.

13. Direction of the first harmonic as a function of time and Jovicentric distance. Note that the scale on the left is different from the scale on the right. The dashed line indicates the regions where the different scales apply.

14. Amplitude of the second harmonic of the 1.2-2.15 MeV proton counting rate as a function of time and Jovian radius.

15. Time histories of proton count rates at two different energies for the near-periapsis period. 15 minute averages of angular distributions are also shown plotted at the center of the 15-minute periods. Locations of orbital crossings of Io and Europa are indicated.

A1. Representative correction curves for count-rate saturation for two of the LET-II counting rates.

A2. Corrected proton flux time histories for the near-periapsis period at two different energies.

TABLE 1.

DETECTOR CHARACTERISTICS

Detector	Energy/Particle Range
HET	2.1 - 8.0 MeV electrons 20 - 500 MeV/Nuc protons and alphas 40 - 120 MeV/Nuc medium nuclei
LET-I	.4 - 3 MeV/Nuc protons (single parameter analysis) 3 - 21 MeV/Nuc protons and alphas 6 - 40 MeV/Nuc medium nuclei
LET-II	.05 - 2.1 MeV electrons (electron-proton separation above .12 MeV) .2 - 21 MeV protons

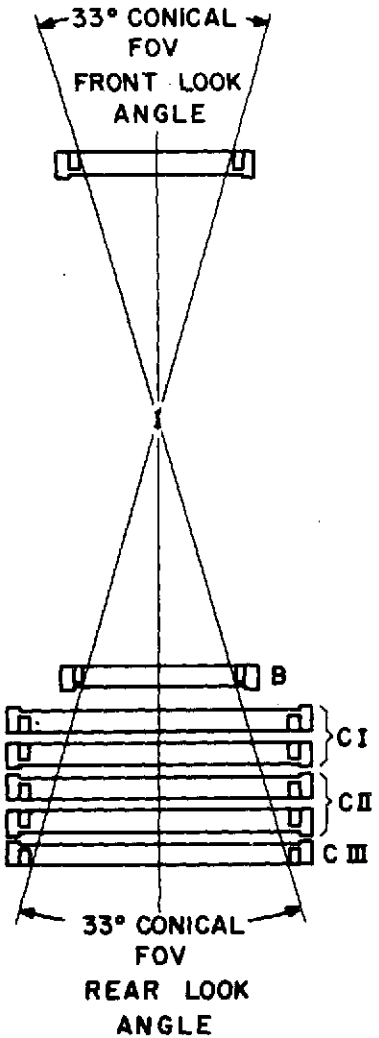

HET TELESCOPE

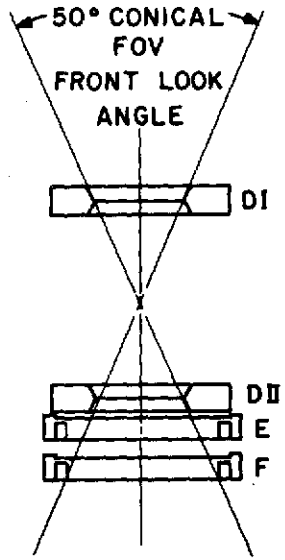

LET-I TELESCOPE

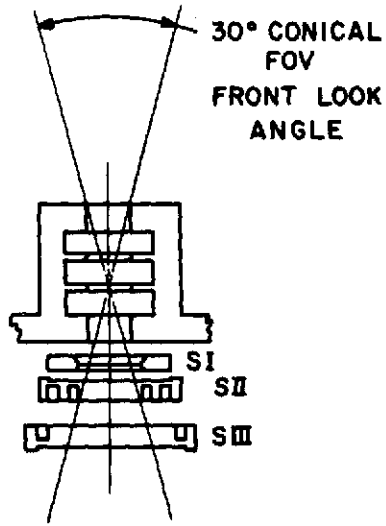

LET-II TELESCOPE

PIONEER F & G DETECTOR COMPLEMENT
COSMIC RAY ENERGY SPECTRA

Fig. 1

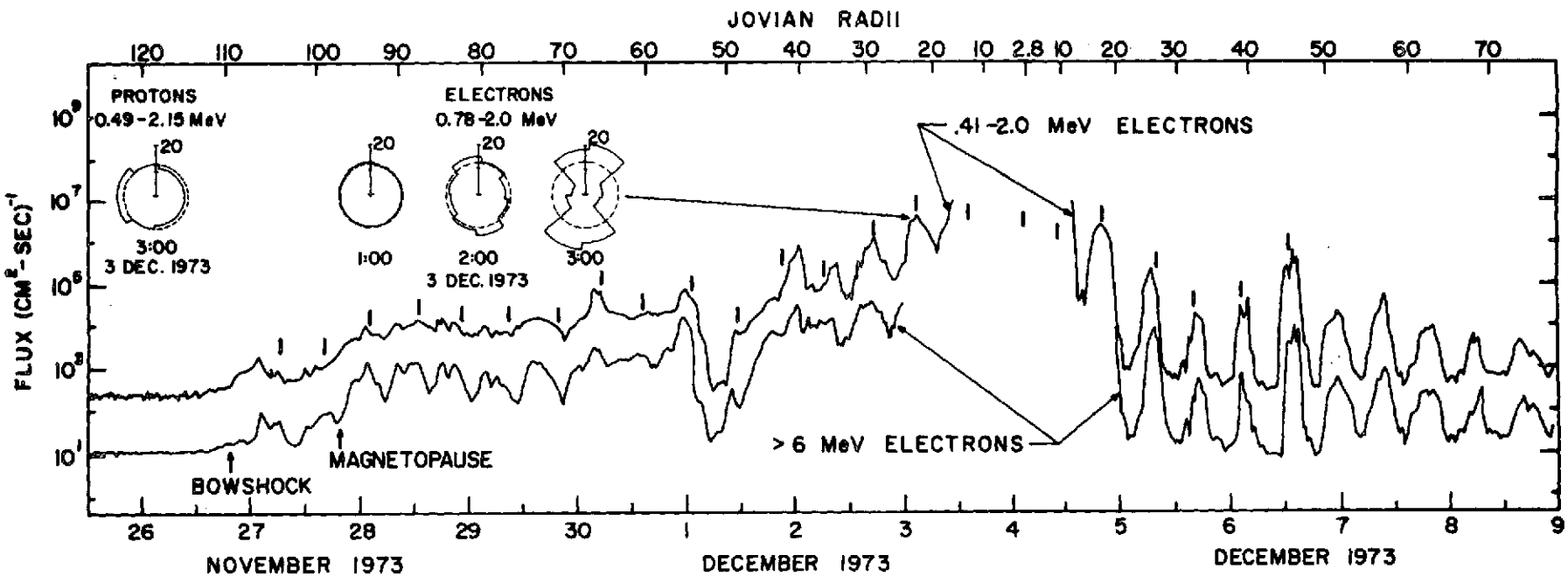
JOVIAN RADII
120 110 100 90 80 70 60 50 40 30 20 10 2.8 10 20 30 40 50 60 70
PROTONS
0.49-2.15 MeV
ELECTRONS
0.78-2.0 MeV
20
3:00
3 DEC. 1973
1:00
2:00
3 DEC. 1973
3:00
.41-2.0 MeV ELECTRONS
>6 MeV ELECTRONS
BOWSHOCK
MAGNETOPAUSE
FLUX (CM²-SEC)⁻¹
10⁹
10⁷
10⁵
10³
10¹
26 27 28 29 30 1 2 3 4 5 6 7 8 9
NOVEMBER 1973
DECEMBER 1973
DECEMBER 1973

Fig. 2

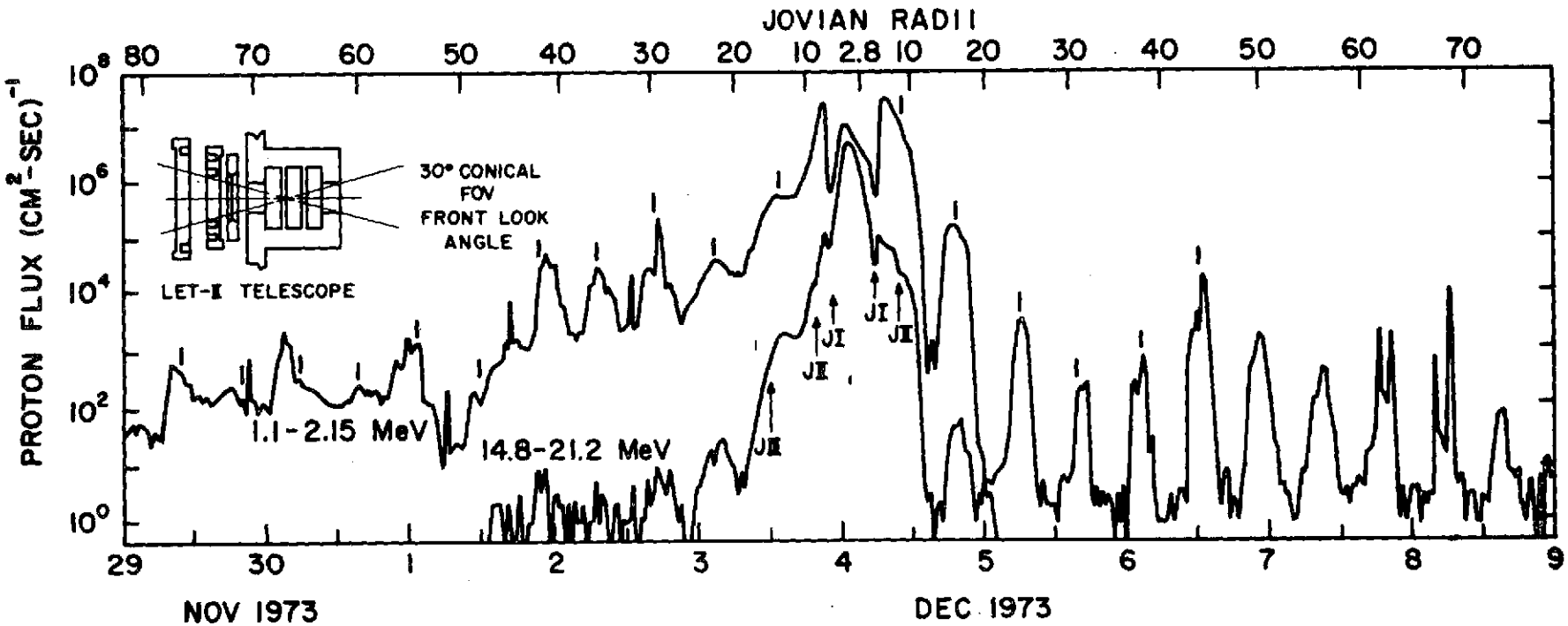
JOVIAN RADII
80 70 60 50 40 30 20 10 2.8 10 20 30 40 50 60 70
PROTON FLUX (CM²-SEC)⁻¹
10⁸
10⁶
10⁴
10²
10⁰
30° CONICAL FOV FRONT LOOK ANGLE
LET-II TELESCOPE
1.1-2.15 MeV
14.8-21.2 MeV
JII
JI
JII
JI
JII
29 30 1 2 3 4 5 6 7 8 9
NOV 1973
DEC 1973

Fig. 3

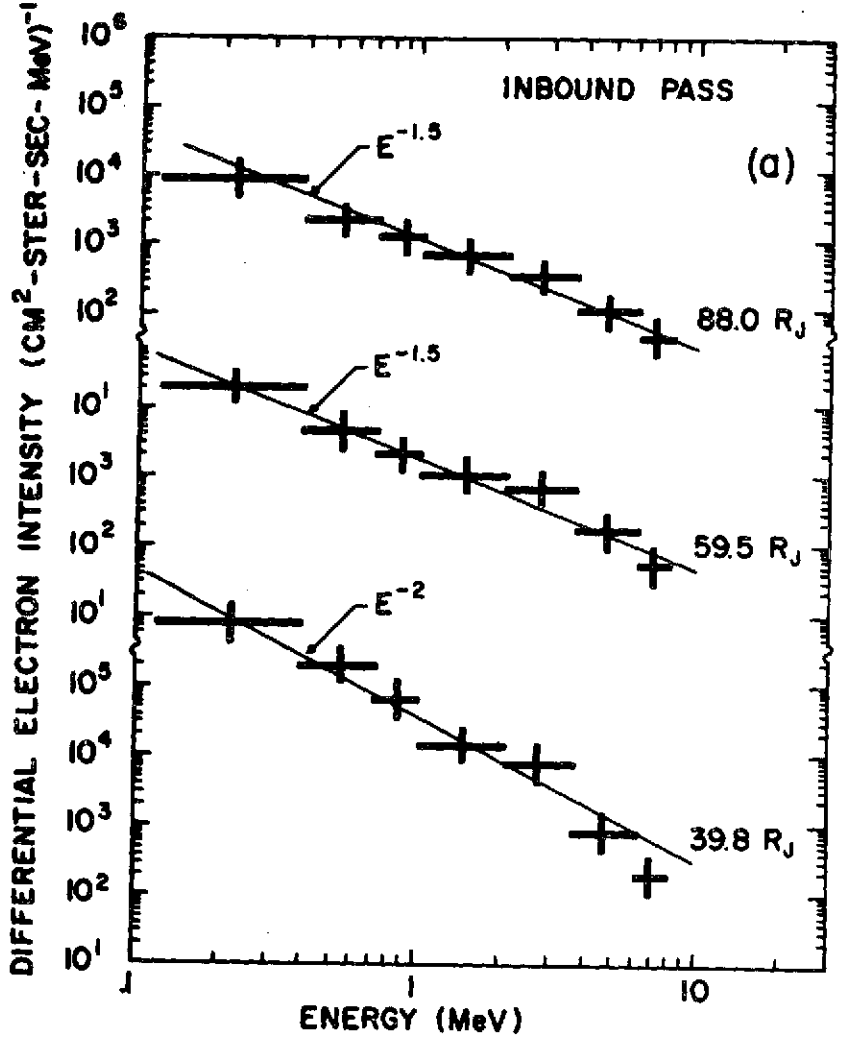
INBOUND PASS
(a)
$E^{-1.5}$
88.0 R_J
$E^{-1.5}$
59.5 R_J
E^{-2}
39.8 R_J
DIFFERENTIAL ELECTRON INTENSITY (CM^2-STER-SEC-MeV)$^{-1}$
ENERGY (MeV)

Fig. 4

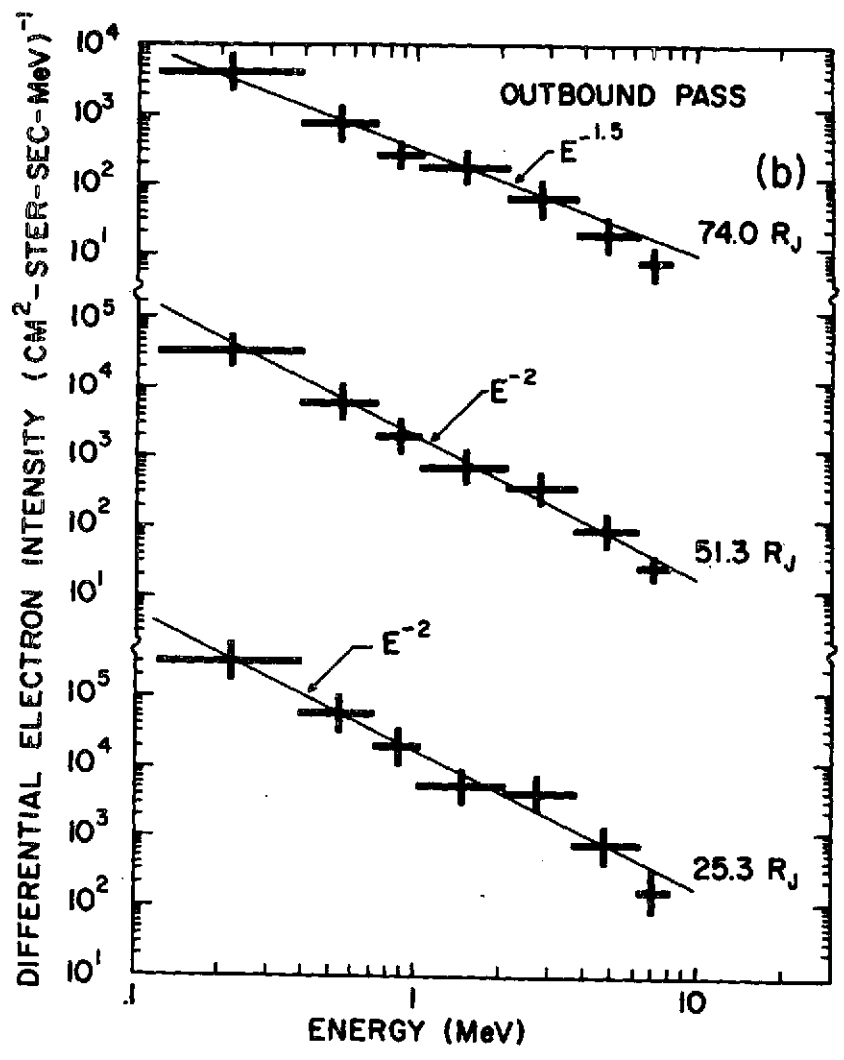
OUTBOUND PASS
(b)
$E^{-1.5}$
74.0 R_J
E^{-2}
51.3 R_J
E^{-2}
25.3 R_J
DIFFERENTIAL ELECTRON INTENSITY (CM^2-STER-SEC-MeV)$^{-1}$
ENERGY (MeV)

Fig. 5

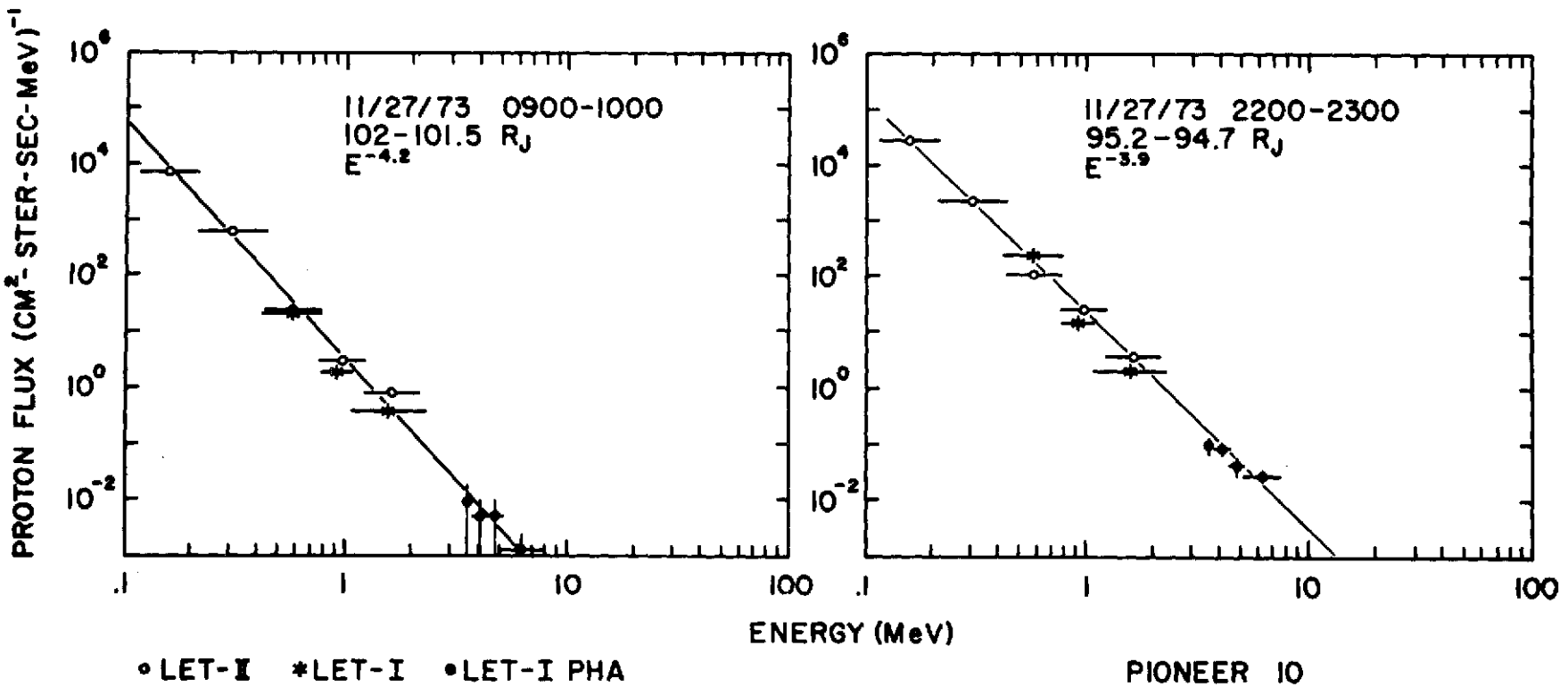
PROTON FLUX (CM²- STER-SEC-MeV)⁻¹
11/27/73 0900-1000
102-101.5 R_J
E^-4.2
11/27/73 2200-2300
95.2-94.7 R_J
E^-3.9
ENERGY (MeV)
∘ LET-II *LET-I •LET-I PHA
PIONEER 10

Fig. 6a

Fig. 6b

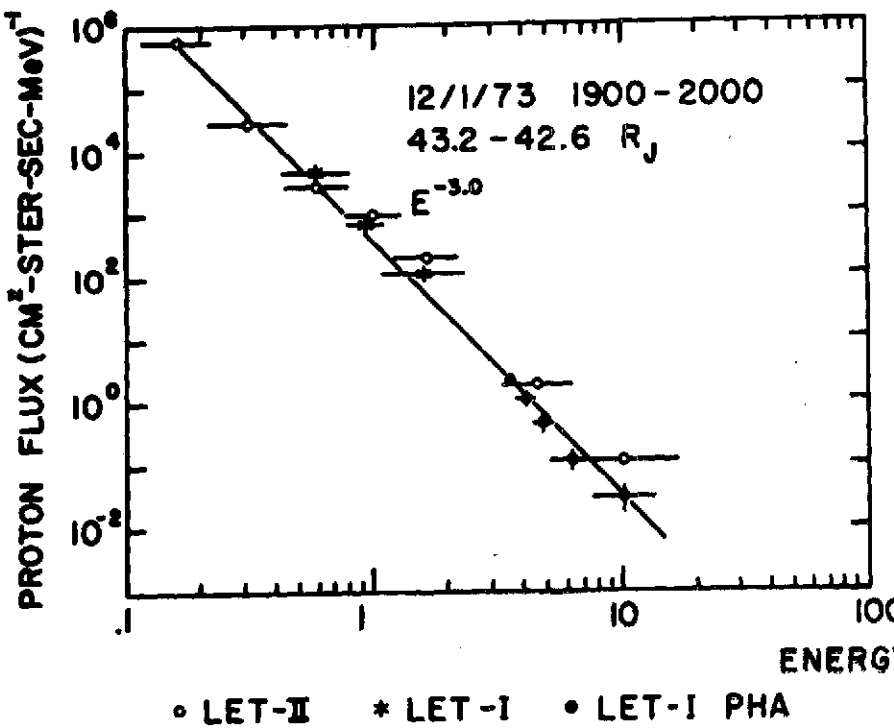
PROTON FLUX (CM²-STER-SEC-MeV)⁻¹
12/1/73 1900-2000
43.2-42.6 R_J
E^-3.0
ENERGY (MeV)
∘ LET-II * LET-I • LET-I PHA

Fig. 6c

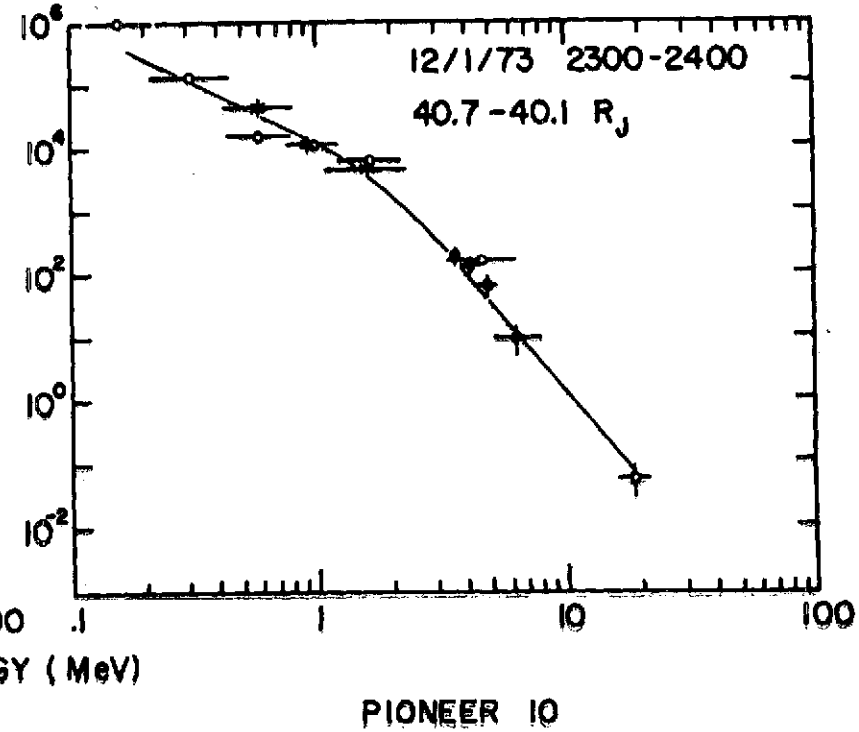
12/1/73 2300-2400
40.7-40.1 R_J
PIONEER 10

Fig. 6d

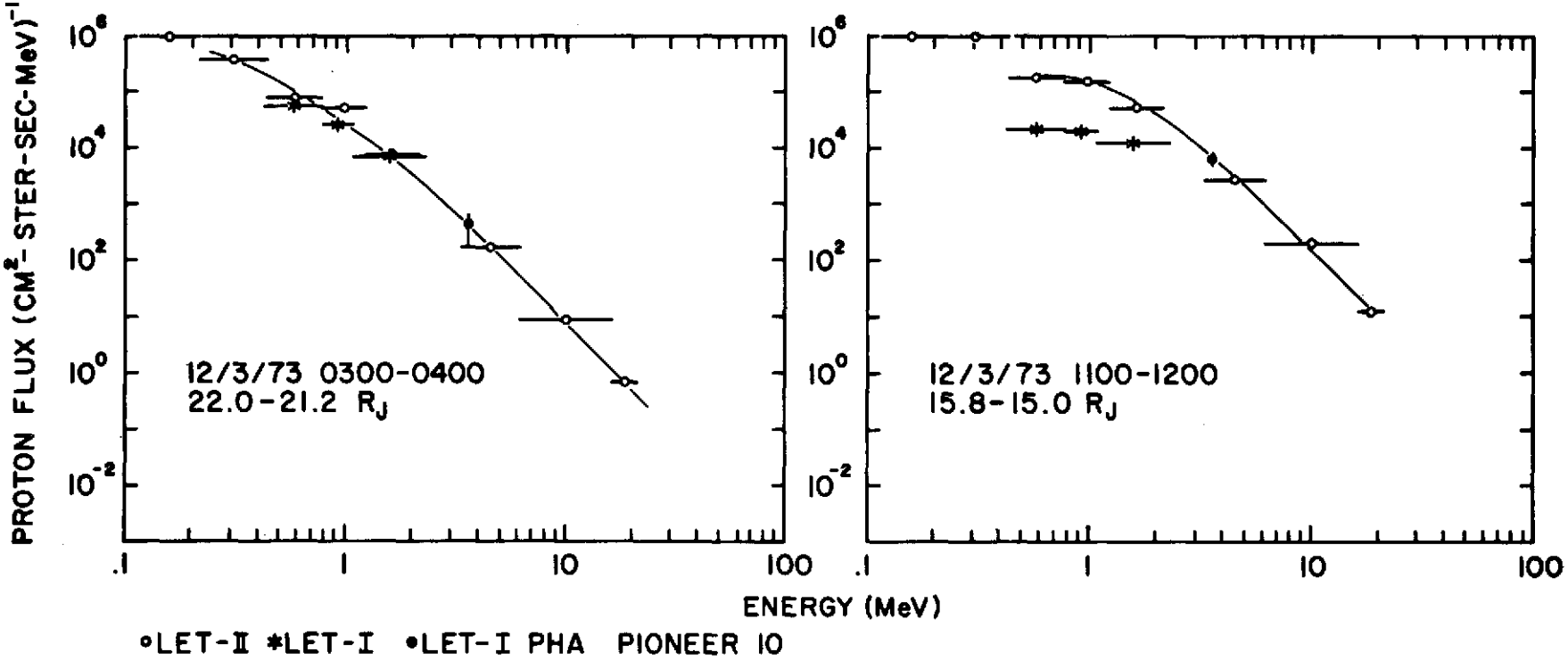
PROTON FLUX (CM²-STER-SEC-MeV)⁻¹
10⁶
10⁴
10²
10⁰
10⁻²
12/3/73 0300-0400
22.0-21.2 R_J
12/3/73 1100-1200
15.8-15.0 R_J
.1
1
10
100
ENERGY (MeV)
°LET-II *LET-I •LET-I PHA PIONEER 10

Fig. 6e

Fig. 6f

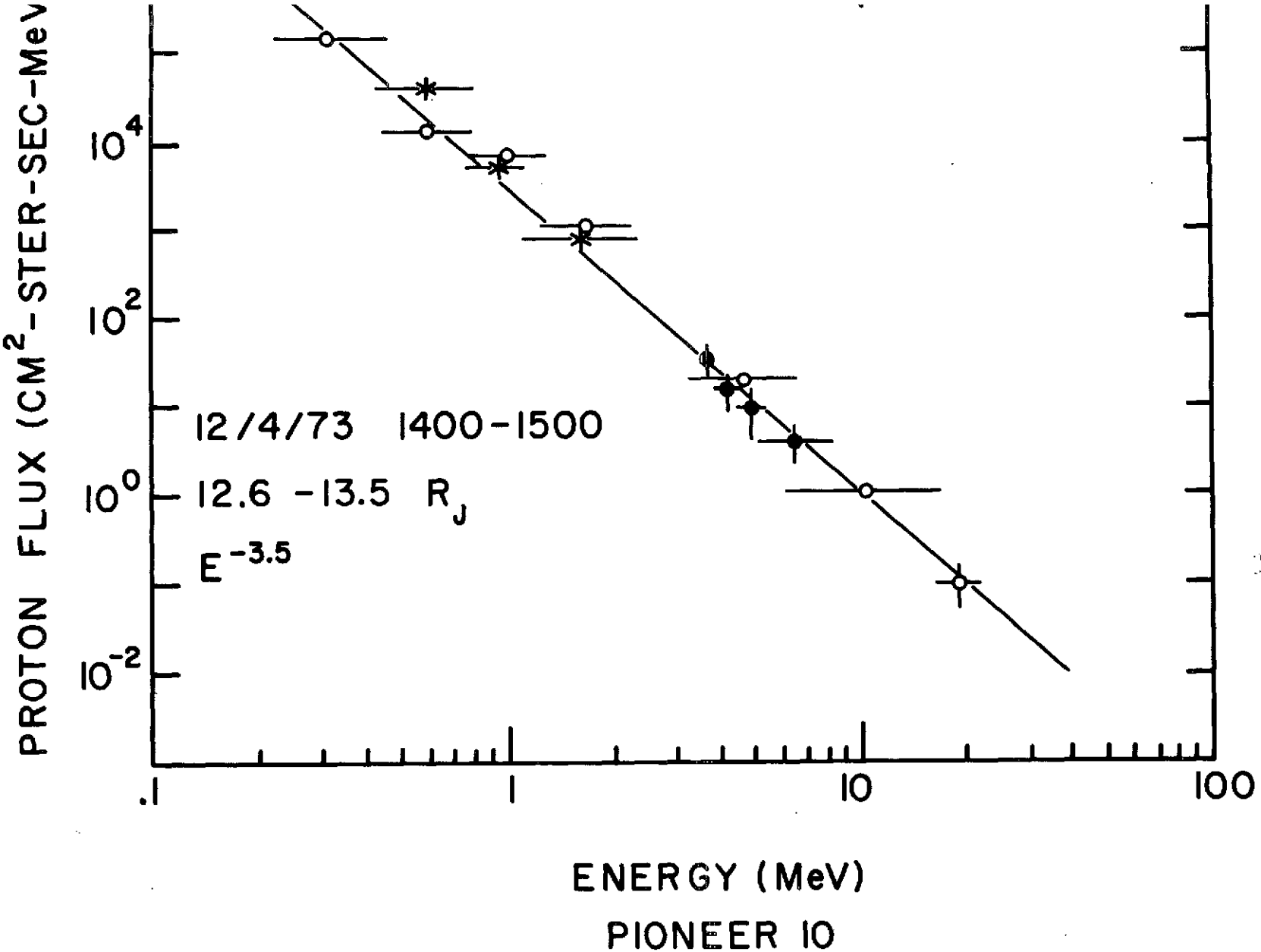
PROTON FLUX (CM^2-STER-SEC-MeV
10^4
10^2
10^0
10^{-2}
12/4/73 1400-1500
12.6 -13.5 R_J
$E^{-3.5}$
.1
1
10
100
ENERGY (MeV)
PIONEER 10

Fig. 6g

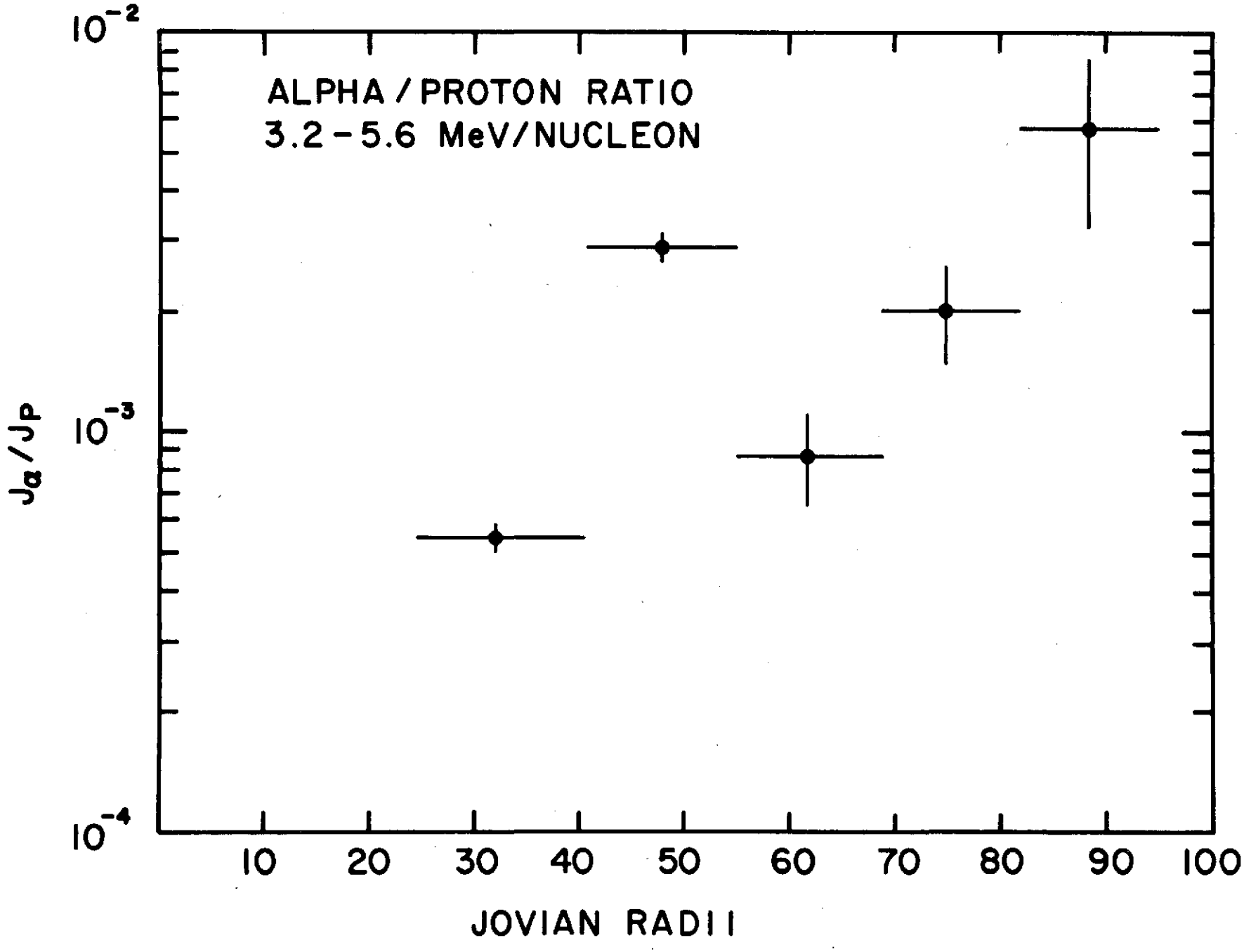
ALPHA / PROTON RATIO
3.2 - 5.6 MeV/NUCLEON
J_α / J_P
10^{-2}
10^{-3}
10^{-4}
10
20
30
40
50
60
70
80
90
100
JOVIAN RADII

Fig. 7

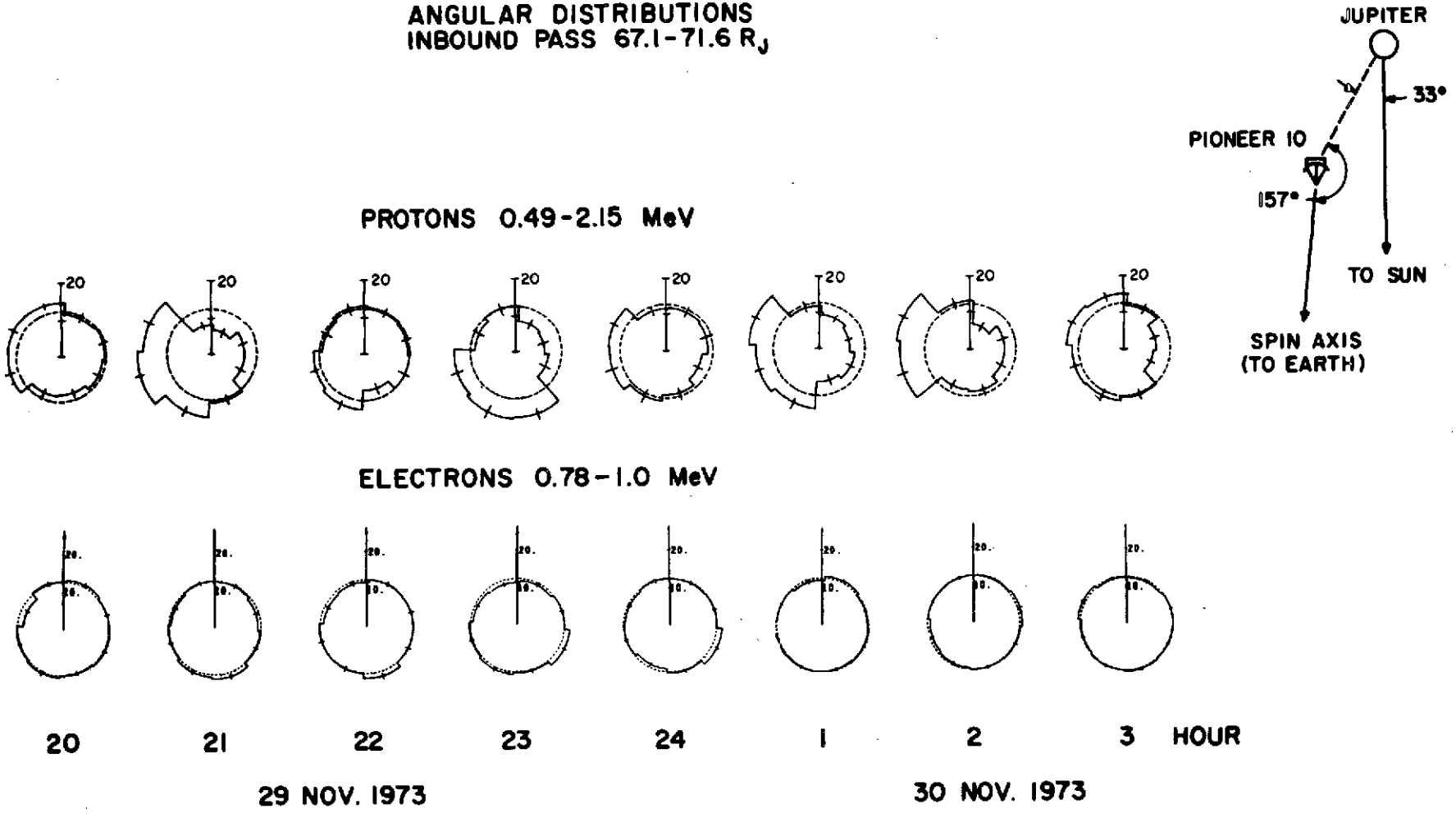
ANGULAR DISTRIBUTIONS
INBOUND PASS 67.1-71.6 R_J
JUPITER
33°
PIONEER 10
157°
TO SUN
SPIN AXIS
(TO EARTH)
PROTONS 0.49-2.15 MeV
20
ELECTRONS 0.78-1.0 MeV
20 21 22 23 24 1 2 3 HOUR
29 NOV. 1973
30 NOV. 1973

Fig. 8

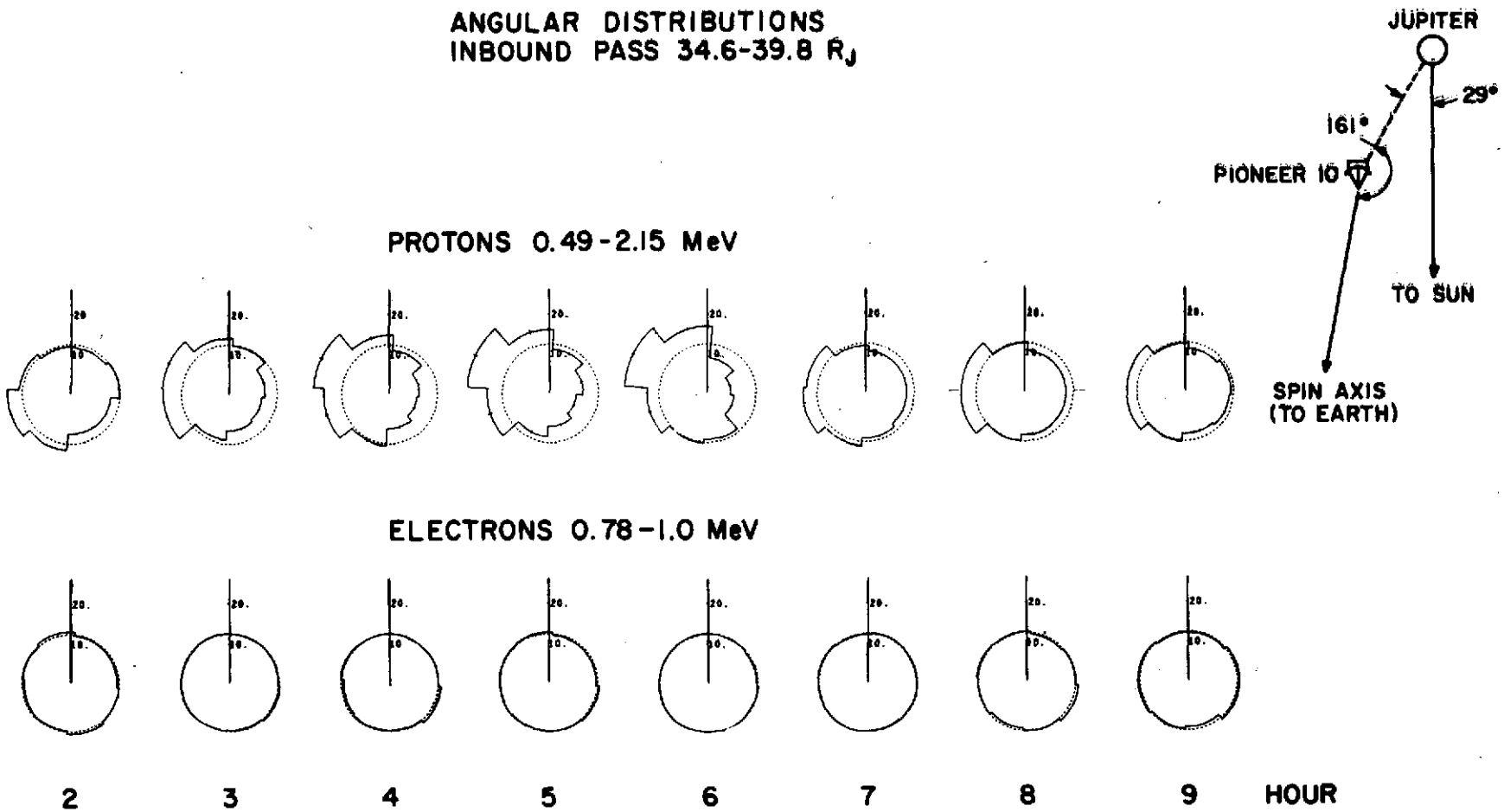
ANGULAR DISTRIBUTIONS
INBOUND PASS 34.6-39.8 R_J
JUPITER
29°
161°
PIONEER 10
TO SUN
SPIN AXIS
(TO EARTH)
PROTONS 0.49-2.15 MeV
ELECTRONS 0.78-1.0 MeV
2
3
4
5
6
7
8
9
HOUR
2 DEC 1973

Fig. 9

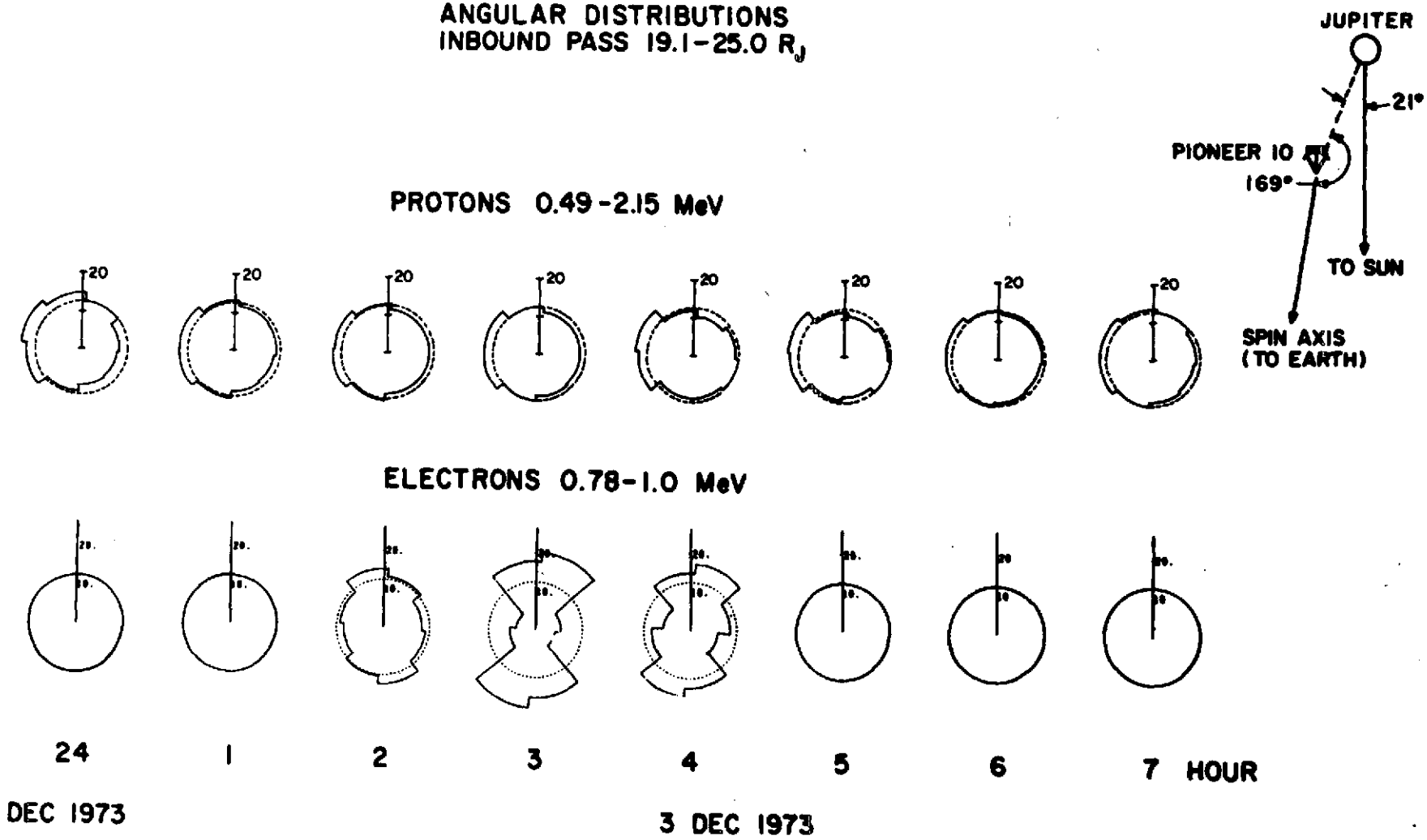
ANGULAR DISTRIBUTIONS
INBOUND PASS 19.1-25.0 R_J
JUPITER
21°
PIONEER 10
169°
TO SUN
SPIN AXIS
(TO EARTH)
PROTONS 0.49-2.15 MeV
20
ELECTRONS 0.78-1.0 MeV
24
1
2
3
4
5
6
7 HOUR
DEC 1973
3 DEC 1973

Fig. 10

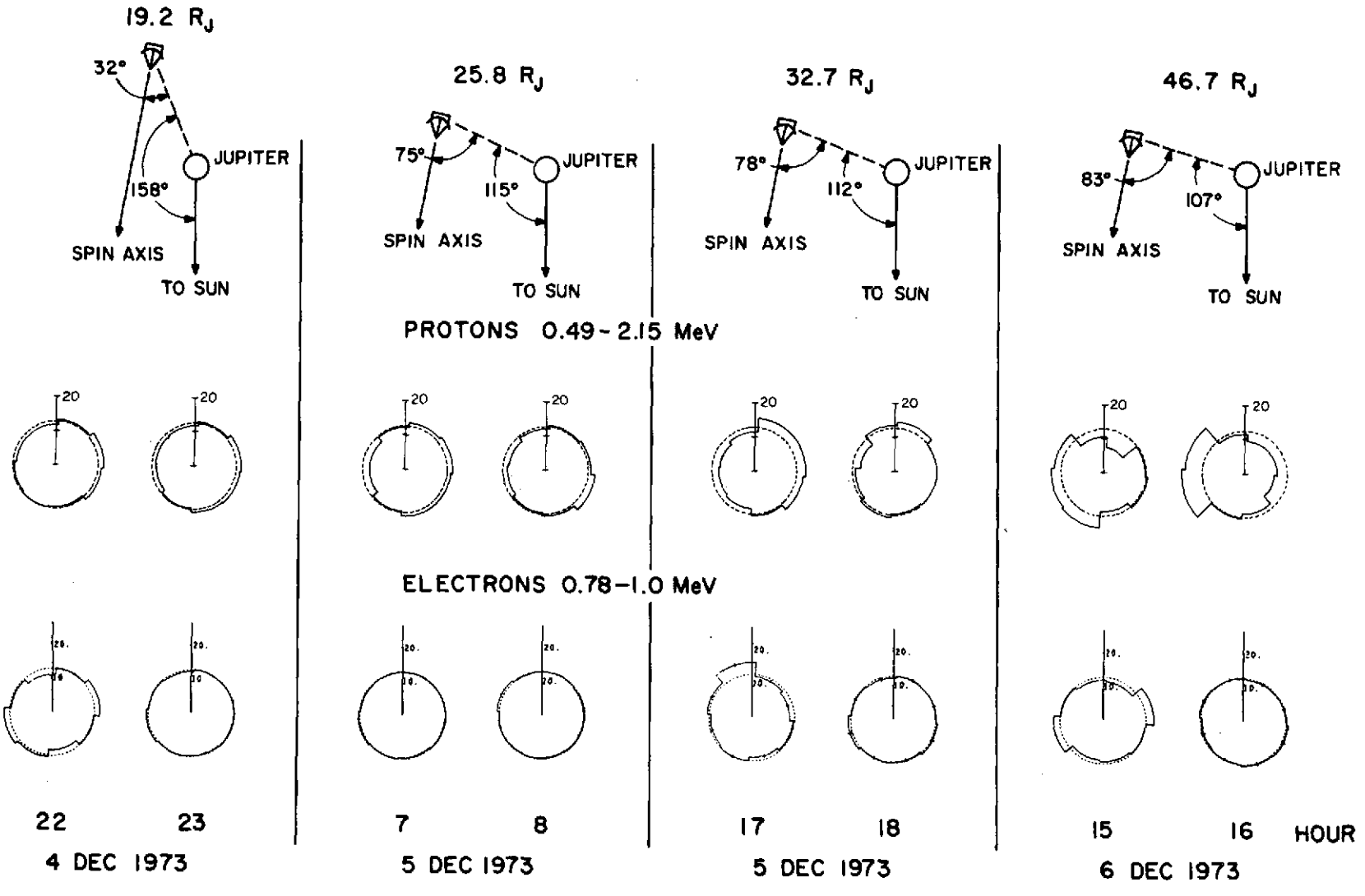
ANGULAR DISTRIBUTIONS
OUTBOUND PASS
19.2 R_J
25.8 R_J
32.7 R_J
46.7 R_J
32°
158°
75°
115°
78°
112°
83°
107°
JUPITER
SPIN AXIS
TO SUN
PROTONS 0.49 - 2.15 MeV
ELECTRONS 0.78 - 1.0 MeV
20
22
23
7
8
17
18
15
16
HOUR
4 DEC 1973
5 DEC 1973
5 DEC 1973
6 DEC 1973

Fig. 11

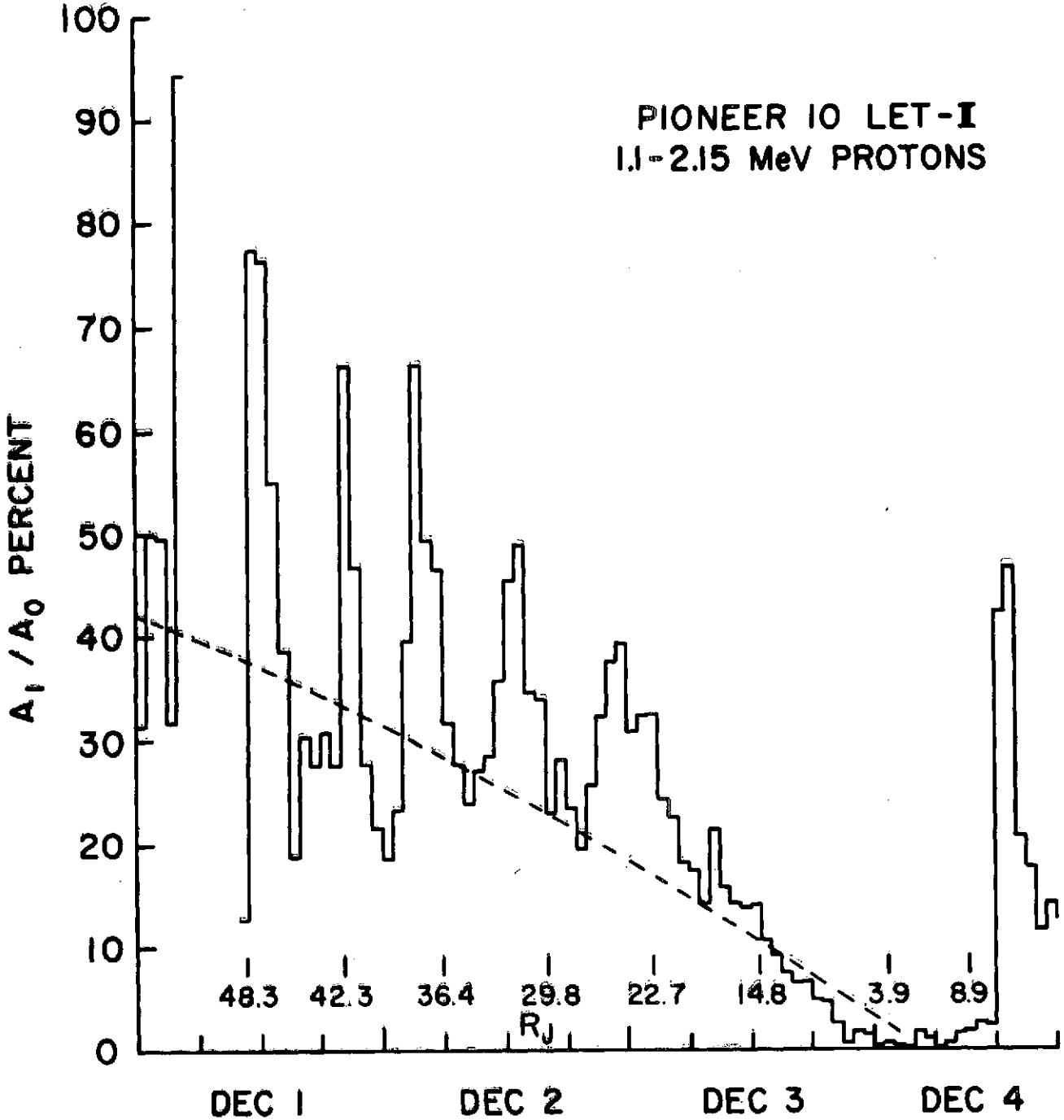
PIONEER 10 LET-I
1.1-2.15 MeV PROTONS
A_1 / A_0 PERCENT
100
90
80
70
60
50
40
30
20
10
0
48.3
42.3
36.4
29.8
22.7
14.8
3.9
8.9
R_J
DEC 1
DEC 2
DEC 3
DEC 4

Fig. 12

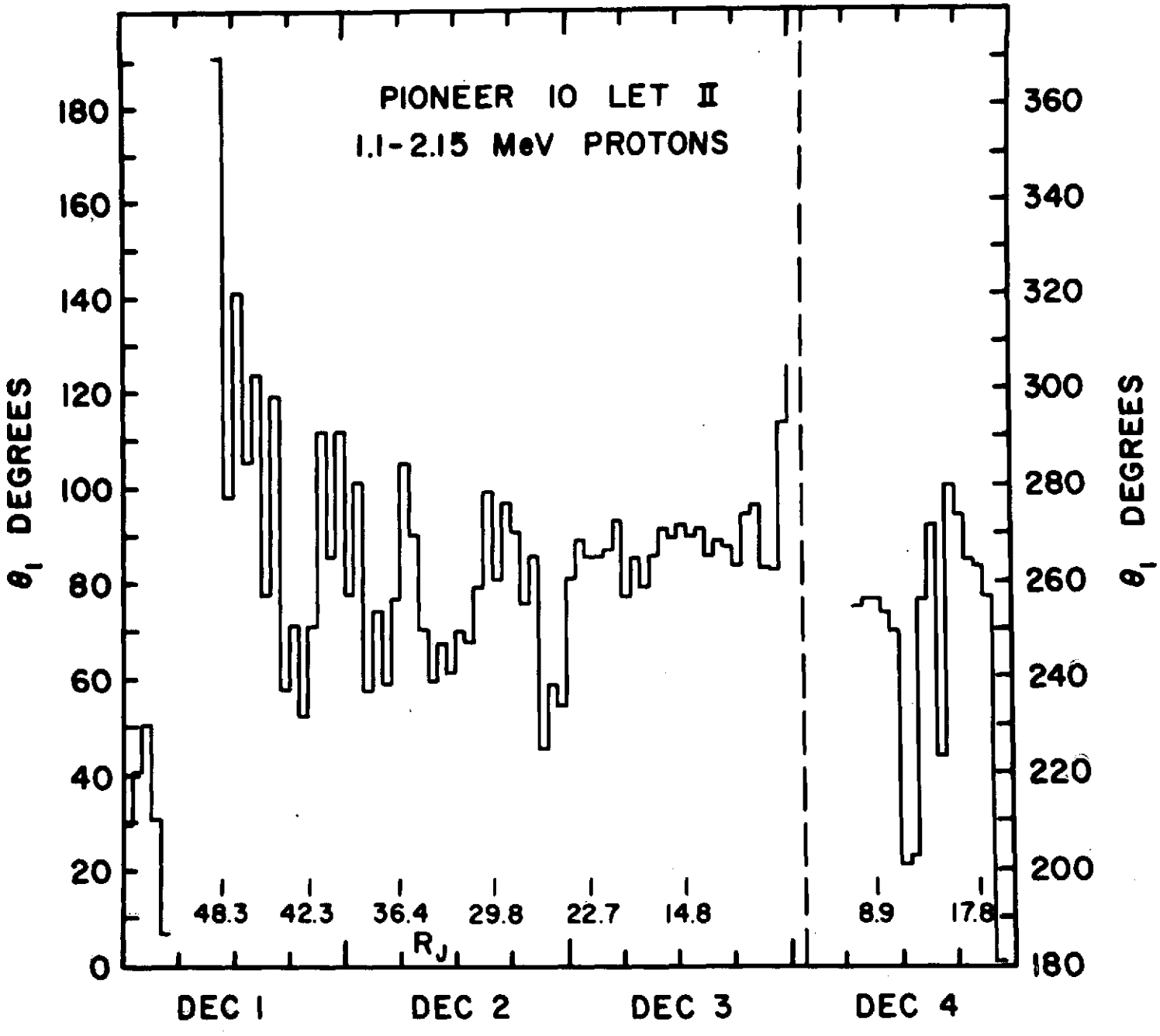
PIONEER 10 LET II
1.1-2.15 MeV PROTONS
θ1 DEGREES
θ1 DEGREES
180
160
140
120
100
80
60
40
20
0
360
340
320
300
280
260
240
220
200
180
48.3
42.3
36.4
29.8
22.7
14.8
8.9
17.8
RJ
DEC 1
DEC 2
DEC 3
DEC 4

Fig. 13

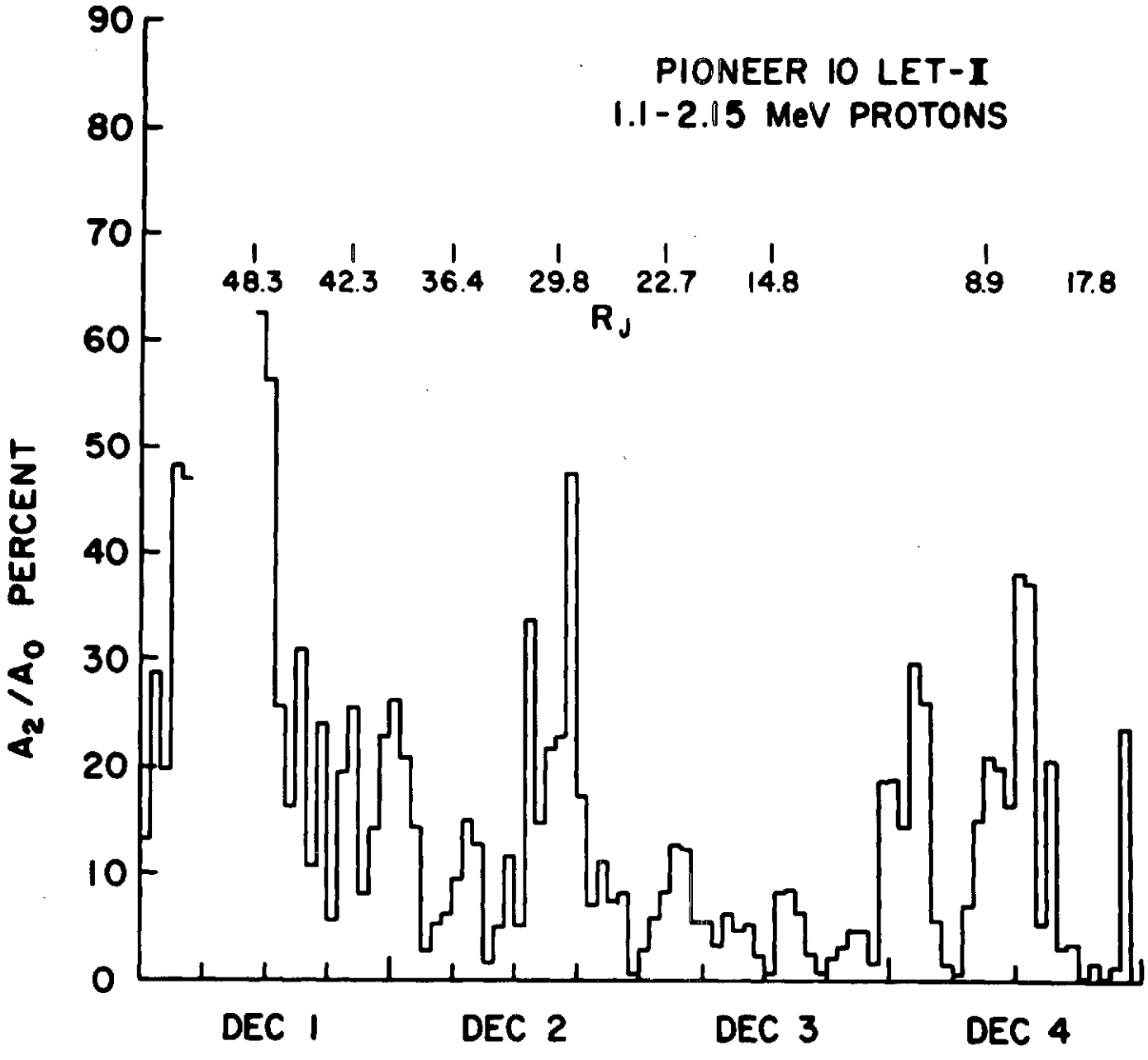
PIONEER 10 LET-I
1.1-2.15 MeV PROTONS
48.3
42.3
36.4
29.8
22.7
14.8
8.9
17.8
R_J
A_2/A_0 PERCENT
0
10
20
30
40
50
60
70
80
90
DEC 1
DEC 2
DEC 3
DEC 4

Fig. 14

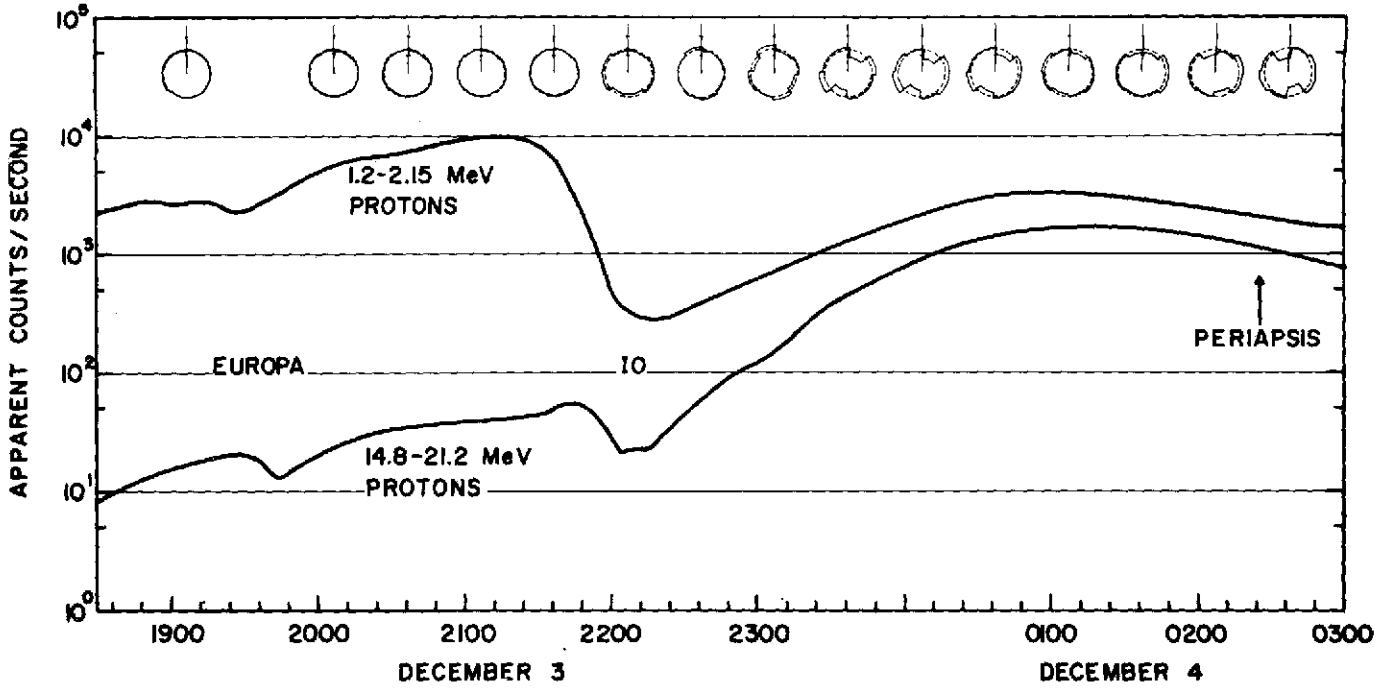
APPARENT COUNTS / SECOND
1.2-2.15 MeV
PROTONS
14.8-21.2 MeV
PROTONS
EUROPA
IO
PERIAPSIS
1900
2000
2100
2200
2300
0100
0200
0300
DECEMBER 3
DECEMBER 4

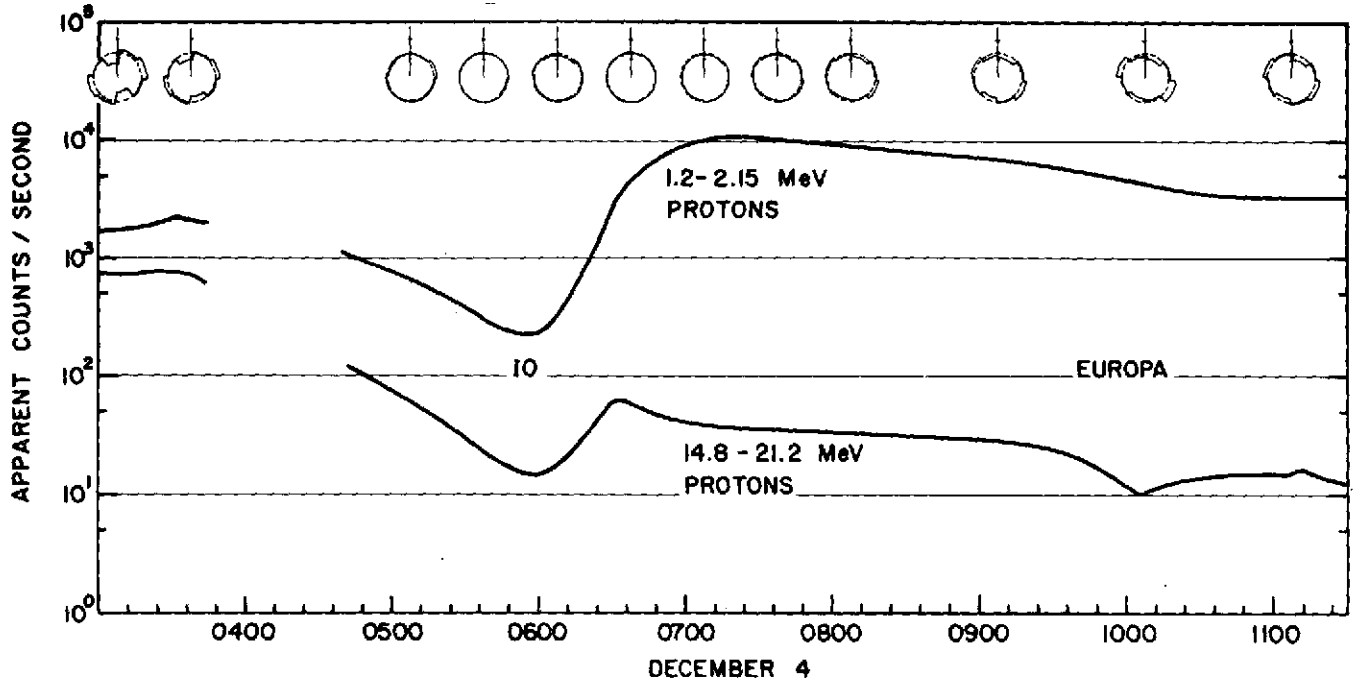
APPARENT COUNTS / SECOND
1.2-2.15 MeV
PROTONS
IO
EUROPA
14.8-21.2 MeV
PROTONS
0400
0500
0600
0700
0800
0900
1000
1100
DECEMBER 4
U.T. AT PIONEER 10

Fig. 15

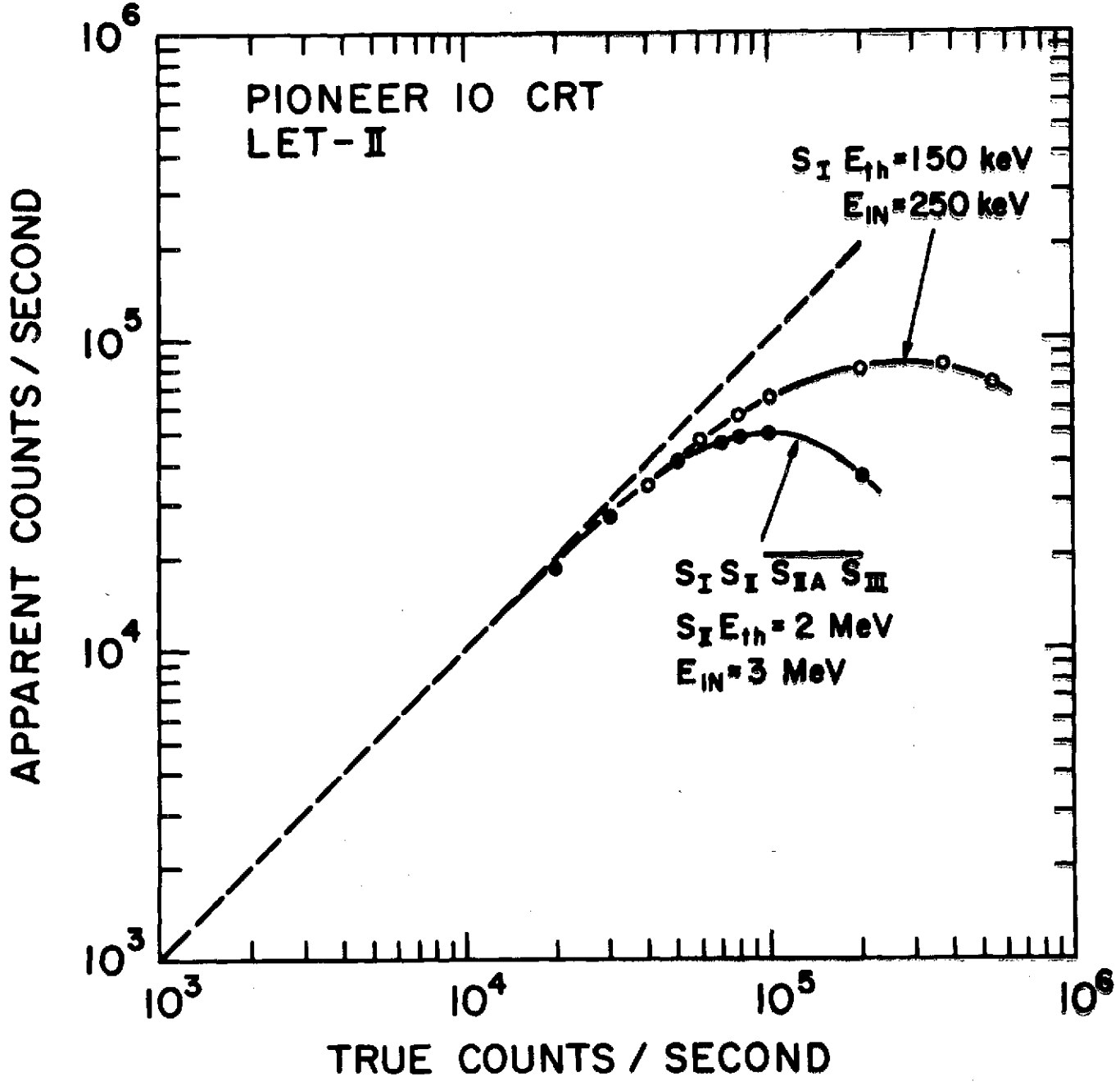
PIONEER 10 CRT
LET-II
S_I E_{th}=150 keV
E_{IN}=250 keV
$S_I S_I \overline{S_{IA}} S_{III}$
$S_I E_{th}$=2 MeV
E_{IN}=3 MeV
APPARENT COUNTS / SECOND
TRUE COUNTS / SECOND
10^3
10^4
10^5
10^6

Fig. A1

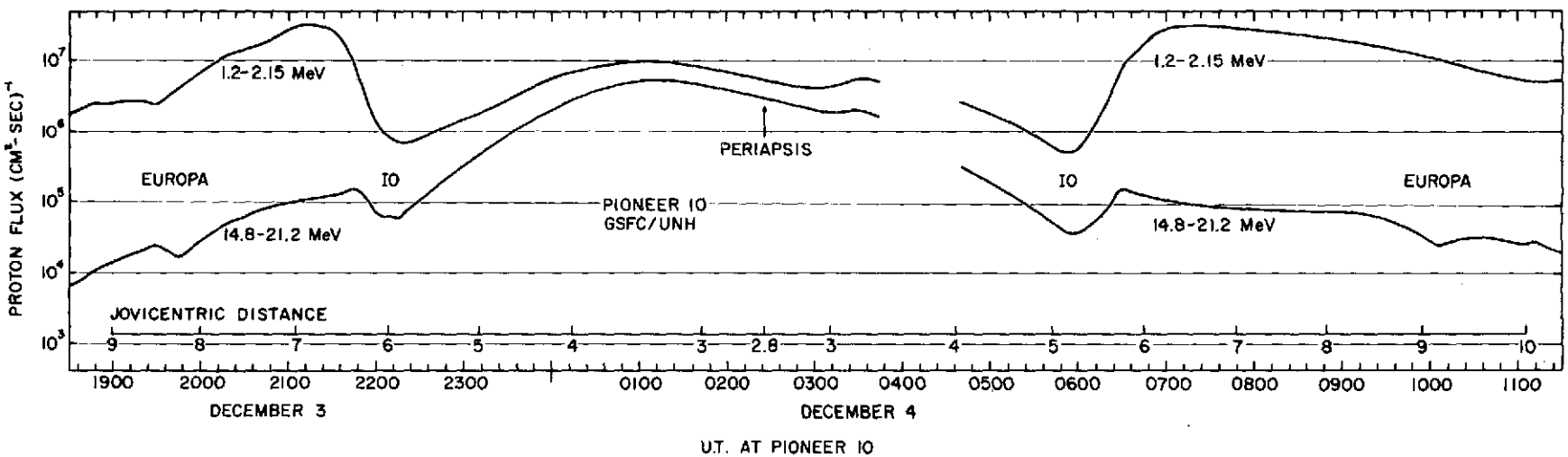
PROTON FLUX (CM²-SEC)⁻¹
10⁷
10⁶
10⁵
10⁴
10³
1.2-2.15 MeV
14.8-21.2 MeV
EUROPA
IO
PERIAPSIS
PIONEER 10
GSFC/UNH
IO
EUROPA
1.2-2.15 MeV
14.8-21.2 MeV
JOVICENTRIC DISTANCE
9 8 7 6 5 4 3 2.8 3 4 5 6 7 8 9 10
1900 2000 2100 2200 2300 0100 0200 0300 0400 0500 0600 0700 0800 0900 1000 1100
DECEMBER 3
DECEMBER 4
U.T. AT PIONEER 10

Fig. A2